incubated with siRNA in a 1:1 ratio for 30 minutes at 22°C. The siPORT amine/siRNA was administered at a total volume of 200 μL. The efficacy of the in vivo transfection was also evaluated by Western blot and reverse transcription–polymerase chain reaction for proteins and genes, respectively (Figure 3). All animal experimental protocols were approved by the animal care and use committee of Fudan University and in compliance with the "Guidelines for the Care and Use

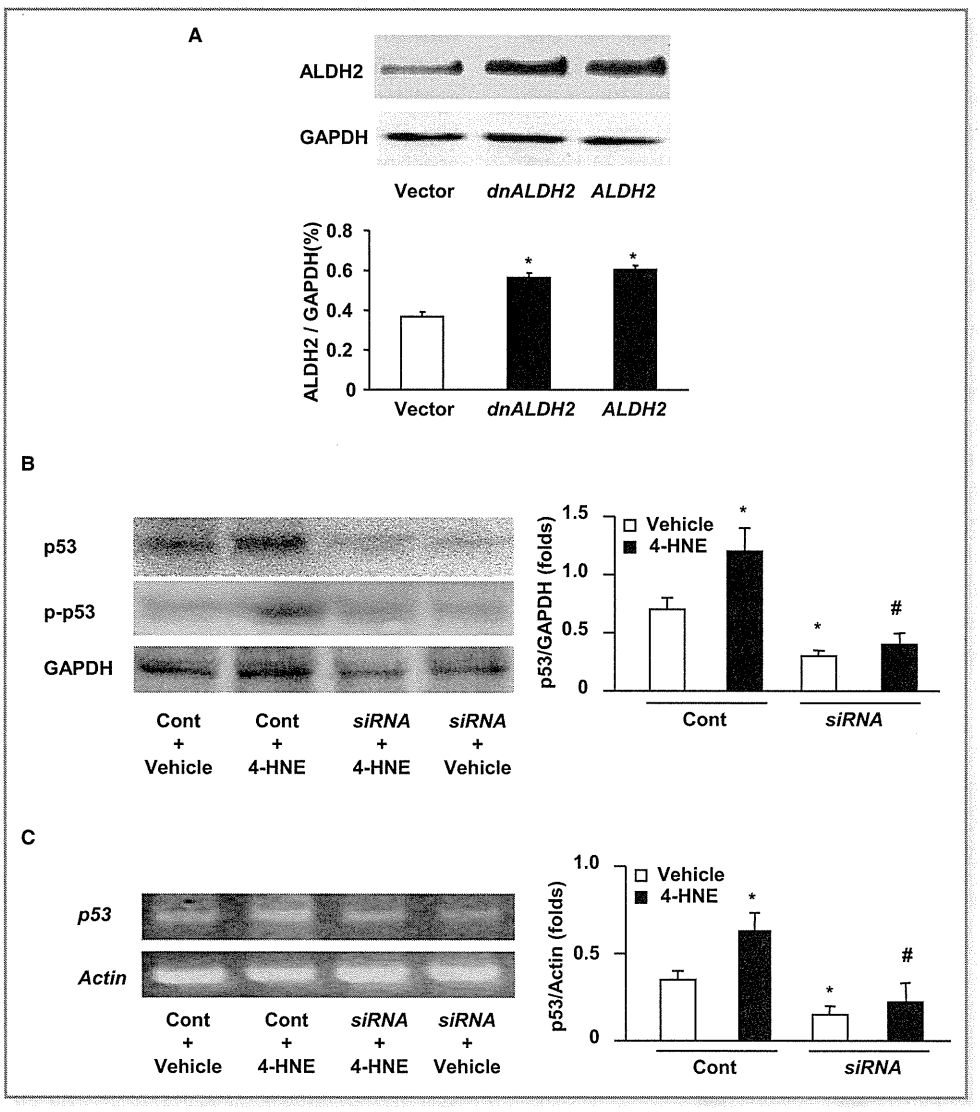

Figure 3. Analysis for cardiac ALDH2 protein expression at 2 days after in vivo gene transfection. A, Mice were subjected to the in vivo gene transfection with *ALDH2*, *dnALDH2*, or empty vector into myocardium. Two days later, the mitochondrial protein from heart tissue was subjected to Western blot analysis for ALDH2 expression. GAPDH was used as a loading control. Representative photographs are shown. Quantification of ALDH2 expression was expressed as folds of GAPDH. Data were shown as mean±SE from 9 samples. *P<0.05 vs vector. B and C, Analysis for p53 expression after treatment with siRNA. *p53* siRNA or a scramble control RNA was injected into wild type mice. The heart was isolated 2 days later and perfused with 4-HNE (10 nmol/L) or vehicle. Total proteins or mRNA from heart tissues of mice were subjected to Western blotting using the anti-p53 and phosphor-p53 antibodies (A) or RT-PCR analysis for the *p53* gene (B), respectively. Representative photographs from 3 independent experiments are shown. GAPDH and β-Actin were used as loading controls. Quantification of p53 expression was expressed as folds of GAPDH or β-Actin. Data were shown as mean±SE from 9 samples. *P<0.05 vs control–vehicle. #P<0.05 vs control–4-HNE. 4-HNE indicates 4-hydroxy-2-nonenal; ALDH2, aldehyde dehydrogenase; Cont, control; dnALDH2, dominant negative forms of *ALDH2*; siRNA, small interefering RNA.

of Laboratory Animals" published by the National Academy Press (NIH Publication No. 85-23, revised 1996).[25]

Induction of MI

MI was induced by persistent ligation of the left anterior descending artery at the same levels in animals: WT and *ALDH2*-KO mice and mice overexpressing ALDH2.[26] Sham animals underwent identical surgical procedures without left anterior descending artery ligation. Ischemic areas were controlled by Nagar-Olsen staining of the hearts at 24 hours after ligation (Figure 4).

2D Gel Electrophoresis

The 2D gel electrophoresis was carried out, first, by isoelectric focusing and, second, by SDS-PAGE. Isoelectric focusing was performed with passive in-gel rehydration of the sample followed by active in-gel rehydration of the sample in 1 dimension. Prior to SDS-PAGE, the immobilized pH gradient strips were equilibrated and sealed at the top of the 2D polyacrylamide vertical-slab precast gels. After separation performed on 12% SDS-PAGE using the Ettan DALT VI apparatus (Amersham Biosciences), the gels were stained with colloidal Coomassie blue and then scanned with an ImageScanner (Amersham Biosciences). The selected spots were sighted for further mass spectrometry identification.

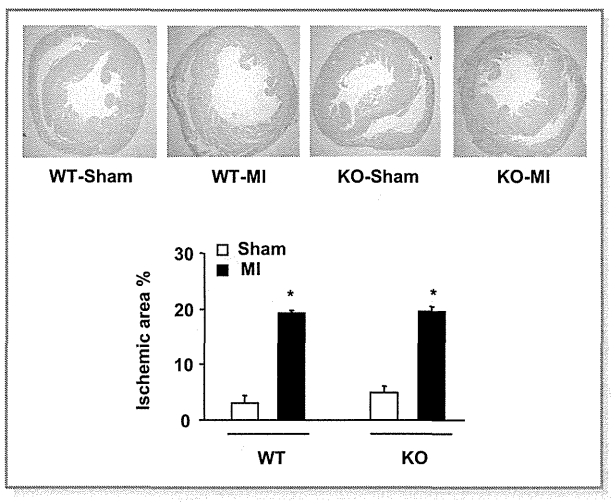

Figure 4. Analysis of ischemic area after 24 hours of MI operation. WT and *ALDH2*-KO mice were subjected to sham or MI operation. After 24 hours, the heart was removed and fixed, and the sections were subjected to Nagar-Olsen staining. Representative photographs were shown. Ischemic area was calculated as a percentage of whole left ventricle section area. Data are shown as mean±SE from 3 hearts (n=3). *P<0.01 vs respective sham-operated mice. ALDH2 indicates aldehyde dehydrogenase; KO, knockout; MI, myocardial infarction; WT, wild type.

Identification of 2D Separated Proteins

Protein spots were excised from Coomassie blue stained gels, washed with MeOH/H_2O and ACN and digested with trypsin overnight at 37°C. For mass spectrometry analysis, the peptides were separated using reverse-phase chromatography. Peptide analysis was performed on an LCQ ion trap mass spectrometer (Image master 6.0, Amersham) equipped with a gold-plated spray capillary. A mass spectrum in full-scan mode was followed by 2 tandem mass spectrometry spectra of the most abundant peptide ions.

Preparation of Human Heart Tissues

Failing human hearts were obtained from 5 end-stage HF patients admitted to our hospital for heart transplantation. Three donor hearts that could not be transplanted for technical reasons were used for controls.

Echocardiography

Echocardiography was performed using an animal-specific instrument (Vevo 770; VisualSonics Inc). Animals were anesthetized by isoflurane, and M-mode images were recorded when the heart rate of the mice was maintained at 450 to 500 beats per minute. LV ejection fraction and LV end-diastolic dimension were measured, as described previously.[21,22,26] All measurements were averaged for 5 consecutive cardiac cycles and were carried out by 3 experienced technicians who were unaware of the identities of the animal groups.

Measurement of LV Pressure

Mice were anesthetized with a cocktail of ketamine HCl (100 ng/kg) and xylazine (5 ng/kg), and the 1.4 F Millar Micro-Tip Catheter Pressure Transducer (Millar Instruments, Inc) was inserted from the right carotid artery into the aorta and then the LV of the mice. The transducer was connected to a Mac Lab system (AD Instruments) to record LV end-diastolic pressure.[21,22,25]

Langendorff Perfusion of Isolated Hearts

Mice were randomly divided into vehicle and 4-HNE perfusion groups.[25] In the vehicle group, hearts were perfused with Krebs-Henseleit buffer for 2 hours; in the 4-HNE group, hearts were perfused with 10 nmol/L 4-HNE in Krebs-Henseleit buffer for 2 hours. The concentration of 4-HNE used for Langendorff perfusion in our present study was determined by

2 steps. First, we analyzed the amount of 4-HNE in homogenizer of hearts isolated from *ALDH2*-KO mice subjected to MI for 4 weeks, and we calculated the concentration of 4-HNE (11.6±1.2 nmol/L). Second, we used 3 concentrations (5, 10, and 20 nmol/L) of 4-HNE to perfuse hearts of WT mice for 30 minutes and analyzed the injury of the heart by Nagar-Olsen staining. Perfusion with 4-HNE at the concentration of 10 nmol/L induced a significant ischemic injury to the heart; in contrast, 4-HNE at 5 and 20 nmol/L resulted slight (<5%) or severe (>50%) ischemia, respectively, neither of which is consistent with the MI experiments in our present study. Consequently, we decided to use the concentration of 10 nmol/L for 4-HNE perfusion experiments. Infarct area, cardiomyocyte apoptosis, and phosphorylation of p53 were evaluated with Nagar-Olsen staining; terminal deoxyribonucleotide transferase–mediated dUTP nick-end labeling, or TUNEL; and immunohistochemistry and Western blotting, respectively.

Cell Culture, Transfection, Anoxia, and Hypoxia Models

Cardiomyocytes were obtained from the LVs of 1-day-old neonatal rats and cultured in 60-mm dishes at a density of 1×10^5 cells/cm^2 in Dulbecco's modified Eagle's medium supplemented with 10% fetal bovine serum, as described elsewhere.[21,22,26,27] Construction and transfection of ALDH2 cDNA in adenovirus vectors were performed, as described previously.[21,22,26,28,29] Anoxia experiments were carried out by placing the cells in an anoxic incubator (GENbox; bioMérieux) for 30 minutes, 2 hours, 4 hours, and 24 hours (95% N_2 and 5% CO_2). Hypoxia experiments were performed by incubation of cultured cardiomyocytes in a hypoxic incubator (Model 9200; Wakenyaku) with 1% O_2, 5% CO_2, and 94% N_2 at 37°C for 2 or 24 hours.

Measurements of Cardiac Mitochondrial ALDH2 Enzymatic Activities

Mitochondrial fractions were obtained by a method of grade centrifugation. In brief, myocardial tissues or cultured cardiomyocytes were washed by PBS twice, then homogenized and centrifuged at 900*g* for 5 minutes to collect the supernatant. The supernatant was resuspensed with mannital-sucrose and further centrifuged at 10 000*g* for 10 minutes to collect the precipitated mitochondria. The purity of mitochondria evaluated by observation under an electronic microscope was 90% to 95%. The mitochondrial protein concentration was determined with BSA protein assay reagent. As described previously,[20] ALDH2 activity was determined by measuring the initial rate of NADH production at 340 nm using spectrophotometric assay on a spectrophotometer (Beckman) equipped with a kinetics software module. Only the linear portion of the ALDH activity curve was used for enzymatic activity analysis.

Histology

Heart tissues from the ischemic region were fixed in 10% formalin and embedded in paraffin or frozen in liquid nitrogen; sectioned at 4-μm thickness; and stained with Masson trichrome, Nagar-Olsen, and immunohistochemical methods using anti-p53 (#2524; Cell Signaling Technology), phosphor-p53 (FL-393, #sc-6243), poly-(APD-ribose) polymerase (PARP) and 4-HNE antibodies (Santa Cruz Biotechnology Inc). The immunostaining of p53 was performed according to the immunohistochemistry protocol from Cell Signaling Technology using the p53 antibody diluted by 1:2000. To confirm the specific staining for p53 and phosphor-p53, we also stained heart tissues of p53 knockout mice (kindly provided by Dr. Xuemei Tong at Shanghai Jiaotong University, Shanghai, China) using the similar p53 and phosphor-p53 antibodies (Figure 5). Digital photographs were taken at magnification ×20, ×100, or ×400, and 5 random high-power fields from each section were chosen and quantified in a blinded manner. Infarct size, ischemic cardiomyocytes, p53, phosphor-p53, PARP, and 4-HNE were measured in 5 sections from each heart, and the mean value was expressed.

Analyses of Apoptosis

Apoptosis was evaluated by TUNEL assay and fluorescence-activated cell sorting (FACS). TUNEL analyses for ischemic tissue or cultured cardiomyocytes were performed according to the manufacturer's protocol (In Situ apoptosis detection kit; Takara). FACS analysis for apoptosis was performed as follows: cells were washed with PBS, resuspended in 1X Annexin Binding Buffer (BD PharMingen), and incubated with annexin V-fluorescence isothiocyanate (FITC; BD PharMingen) and propidium iodide. Apoptotic cells were measured by Becton Dickinson FACS 18 Caliber bench-top flow cytometer (Image master 6.0). Apoptosis was also evaluated by a transmission electron microscopy and DNA laddering. For DNA fragmentation, total DNA was extracted from cardiomyocytes using a DNA binding column (BioDev Co), washed twice with rinsing fluid, dried, diluted in Tris-EDTA buffer, and separated by agarose gel. DNA fragments were visualized with ultraviolet light.

Western Blot

Proteins from heart tissues and cardiomyocytes were size fractionated by SDS-PAGE and transferred to Immobilon-P membranes (Millipore). The blotted membranes were incubated with antibodies against ALDH2, p53, phosphor-p53, ERKs,

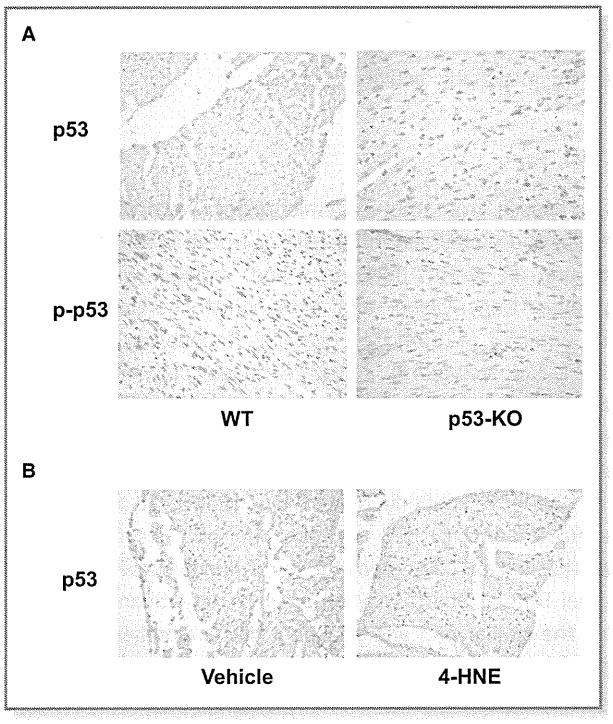

Figure 5. Immunohistochemistry staining of phosphor-p53 and total p53. A, Heart tissues from wild type and p53 knockout mice were fixed in 10% formalin and embedded in paraffin, sectioned at 4-μm thickness, and stained with immunohistochemical methods using anti-p53 and phosphor-p53, respectively. The immunostaining of p53 was performed according to the manufacturer's immunohistochemistry protocol using the p53 antibody diluted by 1:2000. Digital photographs were taken at magnification ×400, and p53 and phosphor-p53 were observed in 5 sections from each heart; the representative photographs are shown. B, Total p53 expression in isolated heart. Isolated hearts were perfused with 4-HNE (10 nmol/L) or vehicle for 2 hours. Representative staining for p53 is shown. 4-HNE indicates 4-hydroxy-2-nonenal; KO, knockout; p-p53, phosphor-p53; WT, wild type.

phosphor-ERKs, JNK, phosphor-JNK, HSP70, or GAPDH (Santa Cruz Biotechnology Inc). Immunoreactivity was detected using an enhanced chemiluminescence reaction system (Amersham Pharmacia Biotech).

Reverse Transcription–Polymerase Chain Reaction

Total RNA was isolated from the LV tissues or cells using TRIzol reagent (15596-018; Gibco BRL). The expression of *ALDH2* and p53 at mRNA levels was evaluated using reverse transcription–polymerase chain reaction. The primers were as follows (forward/reverse): *ALDH2*, agagaggacgcttgctgaac/gcagggcctatcttccaaat; *p53*, 5′-tggctcctccccaacatcttatc-3′/5′-cttcctctgtccgacggtctctc-3′. The polymerase chain reaction products were subject to electrophoresis on 1.5% agarose gels, scanned, and semiquantified using Image-Quant software (Kodak 1D V3.53).

Statistical Analysis

All values are presented as mean±SE. Multiple group comparison was performed by 1- or 2-way ANOVA followed by the Bonferroni procedure for comparison of means. Comparisons between 2 groups were analyzed with the unpaired 2-tailed Student *t* test. Values of $P<0.05$ were considered statistically significant.

Results

Effects of *ALDH2* Modulation on Cardiac Dilation, Dysfunction, and Apoptosis in MI Mice

To elucidate the role of ALDH2 in HF after MI, we produced MI in WT and *ALDH2*-KO mice. *ALDH2*-KO mice showed no significant differences in body weight, blood pressure, heart rate, and echocardiographic parameters compared with WT mice at basal conditions (Table 2). Ischemic injury at early stage (24 hours) after MI was evaluated by Nagar-Olsen staining of the hearts and showed no significant difference between WT and *ALDH2*-KO mice (Figure 4). At 4 weeks after MI, however, the LV cavity, LV end-diastolic pressure, and infarct size were significantly greater and LV ejection fraction was significantly lower in *ALDH2*-KO mice than in WT mice (Figure 6A and 6B). Meanwhile, TUNEL (Figure 6C) and immunohistochemical staining with PARP (Figure 6D) showed that the number of apoptotic cells in the noninfarction LV area was significantly higher in *ALDH2*-KO mice than in WT mice. In contrast, overexpression of *ALDH2* in myocardium of WT mice by injecting adenovirus vectors encoding the murine *ALDH2* gene 2 days prior to MI significantly reduced the LV cavity and LV end-diastolic pressure and increased the LV ejection fraction compared with WT mice injected with empty vector (Figure 7A; Table 3). Infarct size (Figure 7B) and the numbers of TUNEL- or PARP-positive cardiomyocytes (Figure 7C and 7D) were also lower in *ALDH2*-injected hearts than in empty vector–injected hearts. These results collectively suggest that ALDH2 protects against HF after MI partly by reducing cardiomyocyte apoptosis.

Effects of *ALDH2* Modulation on Anoxia-Induced Cardiomyocyte Apoptosis

The effects of *ALDH2* modulation on apoptosis were also observed in cultured cardiomyocytes that underwent anoxia injury. The spectrophotometric assays revealed that the ALDH2 activity of cardiomyocytes was decreased in a time-dependent manner during anoxia (Figure 8A), which was

Table 2. Body Weight, Blood Pressure, Heart Rate, and Echocardiographic Parameters at Basal State

	WT	ALDH2-KO	*P* Value
BW, g	25.9±3.2	26.7±4.0	NS
BP, mm Hg	95.6±6.5	98.1±7.2	NS
HR, bpm	489.3±35.2	494.7±40.5	NS
LVAWd, mm	0.76±0.03	0.78±0.04	NS
LVPWd	0.75±0.04	0.77±0.02	NS
LVESD, mm	1.35±0.18	1.39±0.20	NS
LVEDD, mm	2.97±0.23	3.18±0.41	NS
LVEF, %	80±5.3	81±6.7	NS

Twelve-week-old wild type and ALDH2-KO mice at basal condition were subjected to echocardiographic analysis. Data are shown as mean±SE of 10 mice. ALDH2 indicates aldehyde dehydrogenase2; BP, blood pressure; BW, body weight; HR, heart rate; KO, knockout; LVAWd, left ventricle anterior wall thickness at diastole; LVPWd, left ventricular posterior wall thickness at diastole; LVEDD, left ventricular end-diastolic dimension; LVESD, left ventricular end-systolic dimension; LVEF, left ventricular ejection fraction; NS, not significant.

associated with an increase in apoptosis (Figure 8B). To explore the effects of modulating *ALDH2* on cardiomyocyte apoptosis, an *ALDH2* or *dnALDH2* gene that was constructed by a substitution of Glu with Lys at the 14th last codon of murine *ALDH2*[28] was introduced into cardiomyocytes. ALDH2 activity was significantly decreased in the empty vector–transfected cells after anoxia (Figure 8C), and the decrease of ALDH2 activity was alleviated by *ALDH2* but aggravated by *dnALDH2* transfection (Figure 8C). As expected, anoxia-induced cardiomyocyte apoptosis was attenuated by *ALDH2* but aggravated by *dnALDH2* transfection (Figure 8D). These results suggest that ALDH2 could be a major player in protection of cardiomyocytes from anoxia-induced apoptosis.

Detoxifying the 4-HNE as the Major Mechanism of ALDH2 Effects

4-HNE is one of the most toxic aldehydes produced during lipid peroxidation.[30,31] Because 4-HNE is detoxified by ALDH2, we postulated that 4-HNE might be involved in ALDH2-induced

Table 3. Summary of Echocardiographic Data in Mice Subjected to In Vivo Gene Transfer With Empty Vector or *ALDH2* Into Myocardium and MI for 28 Days

	Vector	*ALDH2*	*P* Value
IVSd	0.4900±0.2074	0.7975±0.2124	0.084
LVIDd	4.2550±0.2356	3.3550±0.5337	0.022
LVPWd	0.8840±0.1168	1.4267±0.3683	0.019
IVSs	0.5767±0.4159	1.5333±0.1935	0.023
LVIDs	3.0200±0.5243	1.4867±0.1537	0.008
LVPWs	1.3650±0.1921	1.7050±0.5092	0.258
RWTs	0.5400±0.2771	1.2667±0.5181	0.099
RWTd	0.2000±0.0361	0.4633±0.1474	0.040
LVVold	81.300±10.629	47.130±17.709	0.016
LVVols	30.478±17.151	5.9900±1.5062	0.061
LV mass uncorrected	102.13±20.929	127.39±29.352	0.174
LV mass corrected	81.702±16.743	101.92±23.472	0.174
LVESD	2.9300±0.5945	1.5750±0.3543	0.008
Stroke volume	49.215±13.028	35.255±4.6366	0.090

Adenovirus vectors encoding *ALDH2* or empty vectors were infused into myocardium of wild type mice. After 2 days, mice were subjected to MI. Echocardiographic analysis was carried out at 4 weeks after MI. Data are shown as mean±SE of 5 mice. ALDH2 indicates aldehyde dehydrogenase 2; IVSd: interventricular septal dimension in diastole; IVSs: interventricular septal dimension in systole; LV, left ventricle; LVIDd, left ventricular internal dimension at end-diastole; LVIDs, left ventricular internal diameter at end-systole; LVESD, left ventricular end-systolic dimension; LVPWs, left ventricle posterior wall thickness at systole; LVV, left ventricular volume; LVVold, left ventricular volume during diastole; LVVols, left ventricular volume during systole; MI, myocardial infarction; RWTd, relative wall thickness at diastole; RWTs, relative wall thickness at systole; Vector, empty vector.

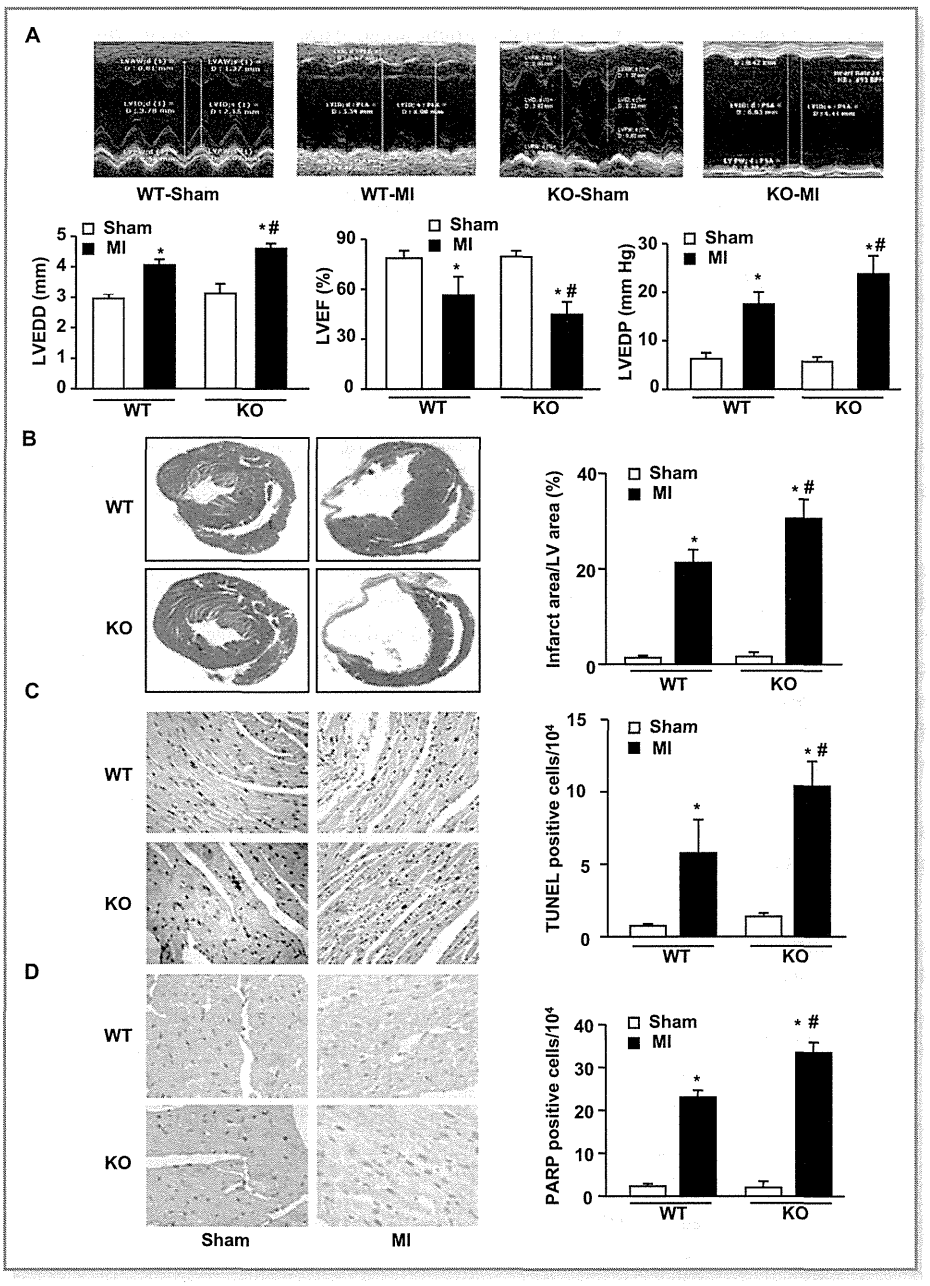

Figure 6. LV dilation, dysfunction, infarct size and cardiomyocyte death after MI in ALDH2-deficient mice. MI was produced in adult male WT and *ALDH2*-KO mice, and LV morphology, function, infarct size, and apoptosis were examined at 4 weeks. A, LV morphology and function. Representative M-mode echocardiographic photographs of LV and quantified LVEDD, LVEF, and LVEDP values are shown. B, Infarct size. Representative photographs of Masson trichrome–stained heart sections from sham-operated and MI mice are shown. Infarcted area was determined by measuring fibrosis area and is expressed as a percentage of the whole LV area. Apoptosis evaluated by TUNEL (C) and immunostaining against PARP (D). Representative photographs are shown. Brown nuclei indicate TUNEL- or PARP-positive cells. Apoptotic cells were counted as the numbers of positive cells per 10^4 cells in the whole LV area. Data are shown as mean±SE from 5 mice. *P<0.05 vs sham in same genotype mice. #P<0.05 vs MI in WT mice. ALDH2 indicates aldehyde dehydrogenase 2; KO, knockout; LV, left ventricle; LVEDD, left ventricular end-diastolic dimension; LVEDP, left ventricular end-diastolic pressure; LVEF, left ventricular ejection fraction; MI, myocardial infarction; PARP, poly-(APD-ribose) polymerase; TUNEL, terminal deoxyribonucleotide transferase–mediated dUTP nick-end labeling; WT, wild type.

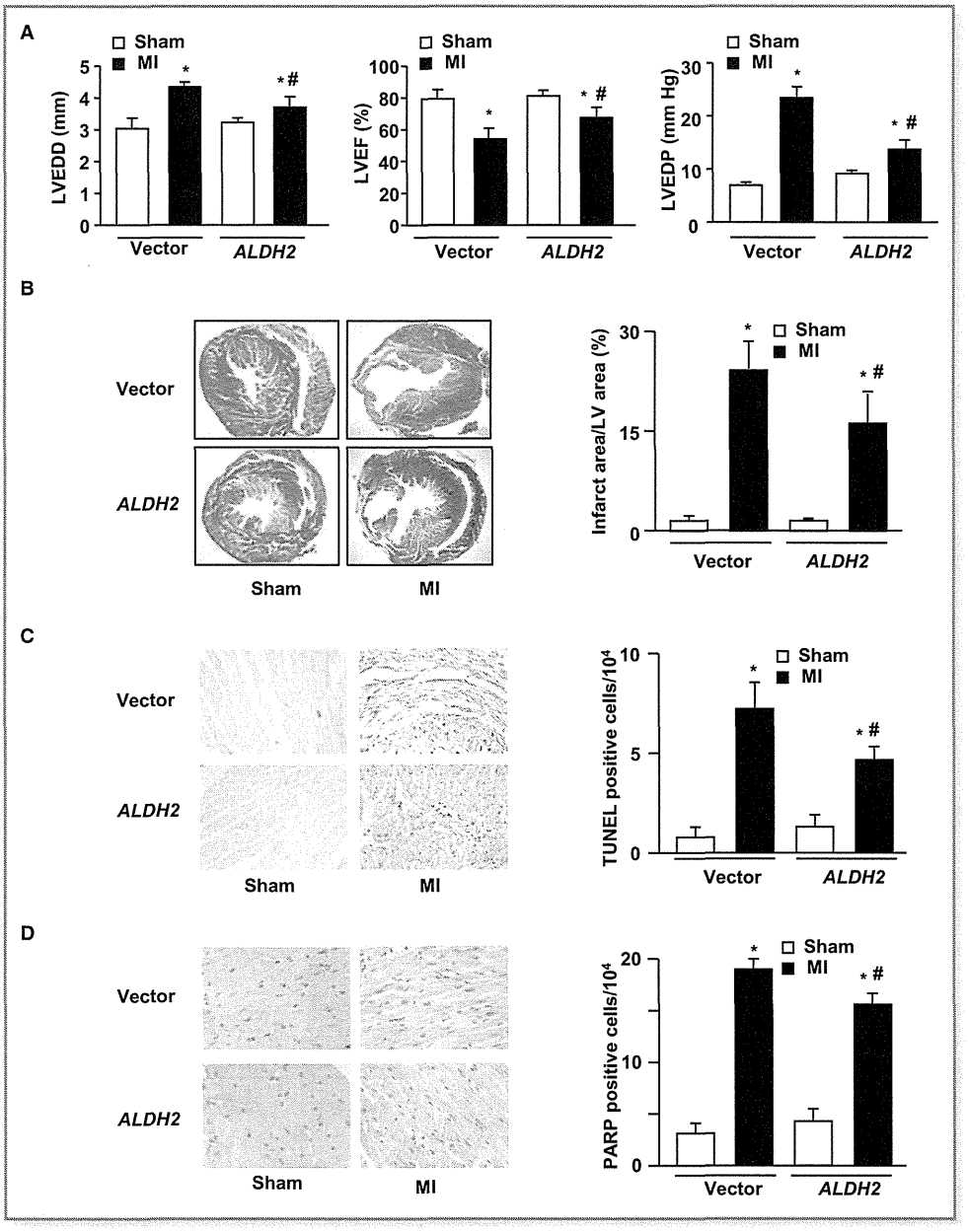

Figure 7. Protection of the heart by overexpression of *ALDH2*. Adenovirus vectors encoding *ALDH2* or empty vectors were infused into myocardium of WT mice. After 2 days, mice were subjected to MI or sham for 4 weeks. A, Quantified LVEDD, LVEF, and LVEDP by echocardiography and catheterization. B, Infarct size. Representative photographs of Masson trichrome staining are shown. TUNEL (C) and immunostaining for PARP (D). Representative photographs are shown. Apoptotic cells were calculated as the numbers of positive cells per 10^4 cells in the whole LV section. Data are shown as mean±SE from 5 hearts. *P<0.05 vs respective sham group, #P<0.05 vs MI mice with vector transfection. ALDH2 indicates aldehyde dehydrogenase 2; LVEDD, left ventricular end-diastolic dimension; LVEDP, left ventricular end-diastolic pressure; LVEF, left ventricular ejection fraction; MI, myocardial infarction; PARP, poly-(APD-ribose) polymerase; TUNEL, terminal deoxyribonucleotide transferase–mediated dUTP nick-end labeling; Vector, empty vector; WT, wild type.

cardiac protection during the development of MI in vivo and in ALDH2-induced antiapoptotic effect on hypoxic cardiomyocytes in vitro.

Our immunohistochemical staining results showed that 4-HNE was almost absent in the LVs of sham-operated WT mice but was readily observed in the border region of infarcted

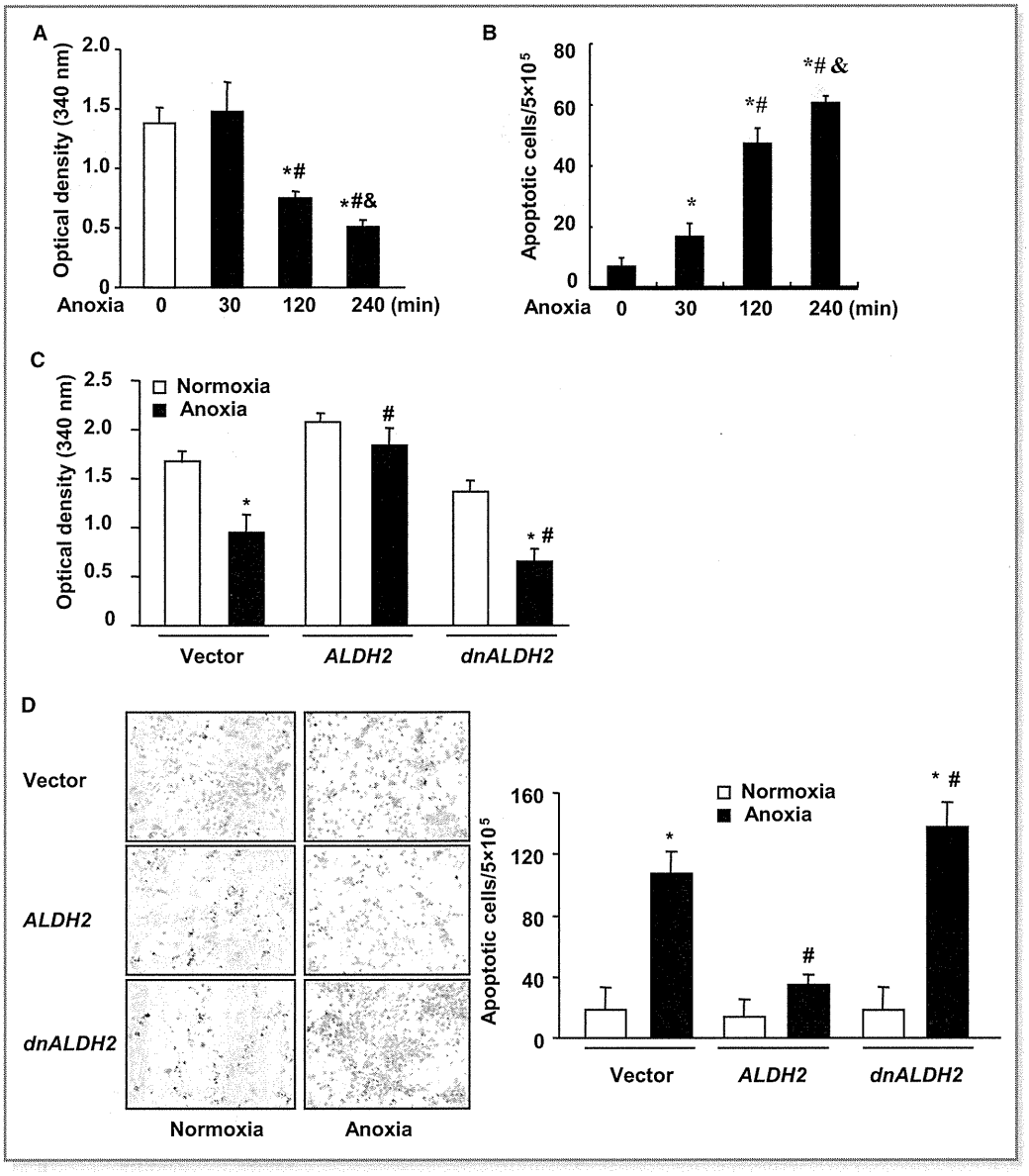

Figure 8. Protection of cultured cardiomyocytes by ALDH2. A, Anoxia-induced changes of ALDH2 activities in cardiomyocytes. Cultured cardiomyocytes were exposed to anoxia for the indicated times. Data are shown as mean±SE from 9 samples. *P<0.05 vs control (0 minute). #P<0.05 vs anoxia for 30 minutes. &P<0.05 vs anoxia for 120 minutes. B, Anoxia-induced apoptosis in cardiomyocytes. Cultured cardiomyocytes were exposed to anoxia for the indicated times. Apoptosis was analyzed by FACS. Data are shown as mean±SE from 9 samples. *P<0.05 vs control (0). #P<0.05 vs treatment with anoxia for 30 minutes. &P<0.05 vs anoxia for 2 hours. C, Effects of *ALDH2* transfection on ALDH2 activities. Cardiomyocytes were transfected with empty vector, *ALDH2* or *dnALDH2* and exposed to anoxia or normoxia for 2 hours. Data are shown as mean±SE from 9 samples. *P<0.01 vs respective normoxia. #P<0.05 vs empty vector with anoxia. D, Effects of *ALDH2* transfection on apoptosis. Cardiomyocytes transfected with empty vector, *ALDH2*, or *dnALDH2* were subjected to anoxia for 24 hours. Apoptosis was detected by TUNEL (brown nuclei). Representative photographs are shown. TUNEL staining was quantified as the number of apoptotic cells per 5×10^5 cells. Data are shown as mean±SE of 9 samples. *P<0.01 vs respective normoxia. #P<0.05 vs vector with anoxia. ALDH2 indicates aldehyde dehydrogenase 2; dnALDH2, dominant negative forms of *ALDH2*; FACS, fluorescence-activated cell sorting; TUNEL, terminal deoxyribonucleotide transferase–mediated dUTP nick-end labeling; Vector, empty vector.

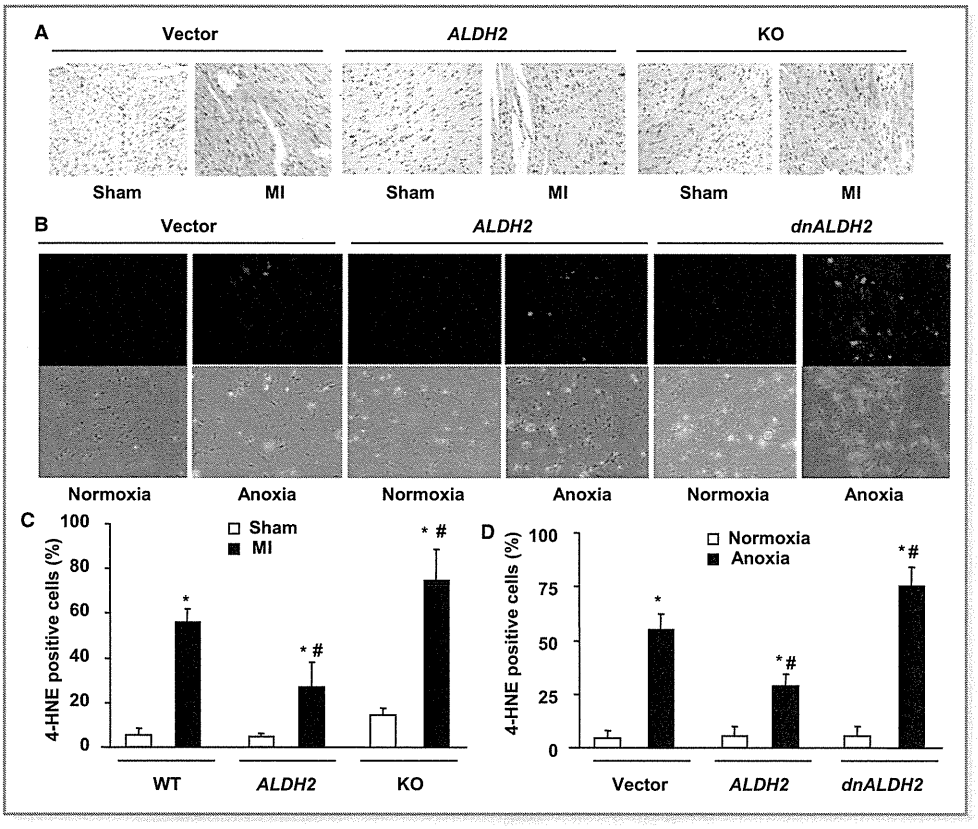

Figure 9. Measurement of 4-HNE in myocardium and cardiomyocytes. A, Distribution of 4-HNE in myocardium. WT mice with cardiac overexpression of *ALDH2* or empty vector and *ALDH2*-KO mice were subjected to MI or sham operation for 4 weeks. 4-HNE was stained with anti 4-HNE antibodies. Representative photographs from 5 hearts are shown. Brown indicates 4-HNE positive signals. B, Detection of 4-HNE in cardiomyocytes. Cultured cardiomyocytes were transfected with *ALDH2*, *dnALDH2*, or empty vector and stimulated with anoxia or normoxia. 4-HNE was detected by immunofluorescent staining method under confocal scanning laser microscopy. Representative photographs are shown. Top, staining of 4-HNE (red). Bottom, cells under the optical microscopy. Quantification of 4-HNE in myocardium (C) and cardiomyocytes (D). 4-HNE–positive cells were presented as percentage of total cells. Data are shown as mean±SE of 5 hearts or 15 cardiomyocytes. *P<0.01 vs respective sham or normoxia. #P<0.05 vs WT with MI or vector with anoxia. 4-HNE indicates 4-hydroxy-2-nonenal; ALDH2, aldehyde dehydrogenase 2; dnALDH2, dominant negative forms of *ALDH2*; KO, knockout; MI, myocardial infarction; Vector, empty vector; WT, wild type.

myocardium of the WT mice (Figure 9A and 9C). The increase in 4-HNE after MI was significantly attenuated by transfection with *ALDH2*. 4-HNE was detectable even in the LVs of sham-operated *ALDH2*-KO mice and upregulated more significantly in the LVs of *ALDH2*-KO mice after MI (Figure 9A and 9C). In cultured cardiomyocytes, anoxia enhanced production of 4-HNE, which was further increased by *dnALDH2* but decreased by *ALDH2* transfection (Figure 9B and 9D), consistent with the changes of cardiomyocyte apoptosis.

These results suggest that the protection of cardiomyocytes by ALDH2 is associated with detoxification of 4-HNE. To observe its direct effects, 4-HNE was perfused into the isolated murine heart in Langendorff mode. Perfusion with 4-HNE induced a significant myocardial injury (Figure 10A and 10B) and apoptosis (Figure 10A and 10C). Furthermore, treatment with 4-HNE significantly induced the karyopyknosis and the DNA fragmentation in cultured cardiomyocytes (Figure 10D and 10E). Taken together, the accumulation of 4-HNE as a consequence of ALDH2 downregulation could induce cardiomyocyte apoptosis, thereby promoting LV dilation and dysfunction after MI.

Involvement of p53 in the Effects of ALDH2 and 4-HNE on Cardiomyocytes

We further examined the potential signaling pathway related to ALDH2-downregulation- and 4-HNE-upregulation-induced cardiomyocyte apoptosis. It is known that the tumor suppressor p53 regulates cardiomyocyte apoptosis and is

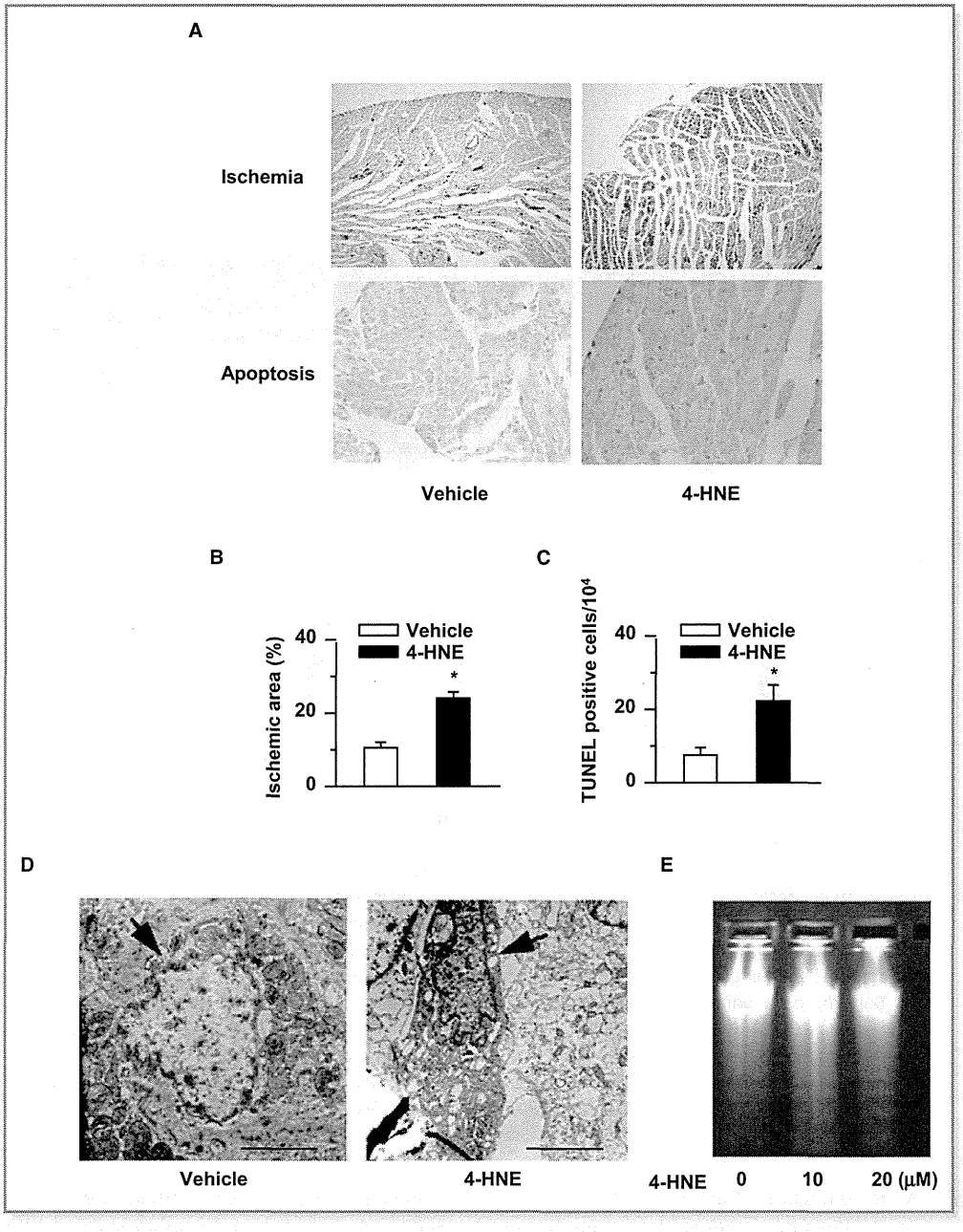

Figure 10. 4-HNE–induced cardiomyocyte injury and apoptosis. A, Myocardial injury and apoptosis induced by 4-HNE. The isolated murine heart was perfused with 4-HNE (10 nmol/L) or vehicle under a Langendorff perfusion system for 2 hours. Ischemic area and apoptosis were analyzed by Nagar-Olsen staining and TUNEL method, respectively. Representative photographs are shown. Top, Nagar-Olsen staining, red signals indicate ischemic area. Bottom, TUNEL, brown nuclei indicate apoptosis. Quantification of ischemic area (B) and apoptosis (C). Ischemic area was calculated as percentage of whole LV area. Apoptotic cells were expressed as the numbers of TUNEL-positive nuclei per 10^4 cells in whole LV area. Data are shown as mean±SE from 5 hearts. *P<0.01 vs vehicle. D, Apoptotic bodies in cultured cardiomyocytes. Cardiomyocytes treated with 4-HNE or vehicle for 24 hours were examined by a transmission electron microscopy. Representative photographs from 9 samples are shown (scale bar = 2 μm). Arrows indicate the nuclei, which showed significant karyopyknosis in 4-HNE- but not vehicle-treated cells. E, DNA fragmentation. Cardiomyocytes were treated with indicated concentrations of 4-HNE for 24 hours. A representative photograph of 9 samples is shown. 4-HNE indicates 4-hydroxy-2-nonenal; LV, left ventricle; TUNEL, terminal deoxyribonucleotide transferase–mediated dUTP nick-end labeling.

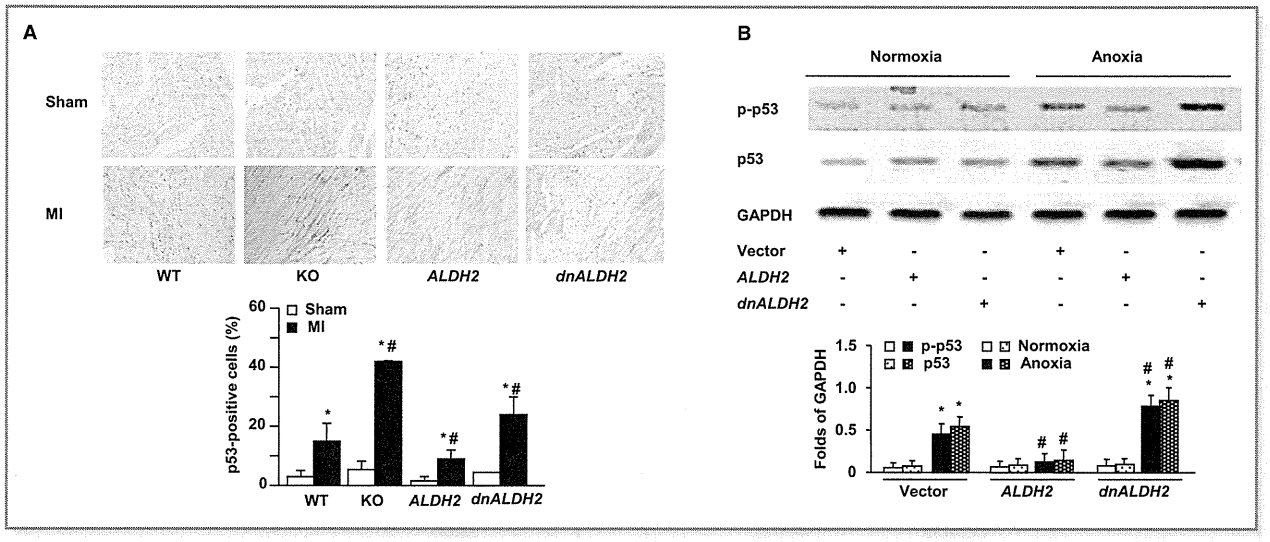

Figure 11. Involvement of p53 in ALDH2- and 4-HNE–induced cardiac injuries. A, Detection of p53 by immunohistochemistry in myocardium. Mice were subjected to sham or MI for 24 hours. p53 was stained by an anti-p53 antibody (brown). Representative photographs are shown. p53 positive cells were calculated in whole LV section and expressed as percentage of total cells. Data are shown as mean±SE of 5 hearts. *P<0.05 vs respective sham. #P<0.05 vs WT with MI. B, Western blot analyses for expression and phosphorylation of p53 in cardiomyocytes. Cultured cardiomyocytes were transfected with empty vector, *ALDH2*, or *dnALDH2* and exposed to anoxia or normoxia for 2 hours (for p-p53) or 24 hours (for p53 protein expression). GAPDH was used as a loading control. Representative photographs are shown. The band densities were determined by scanning each band with a densitometer, and p-p53 and p53 are expressed relative to bands of GAPDH (folds). Data are shown as mean±SE from 15 samples. *P<0.01 vs respective normoxia. #P<0.05 vs empty vector with hypoxia. C, Effects of ALDH2 on phosphorylation and expression of p53 under hypoxia condition. Cultured cardiomyocytes were transfected with empty vector, *ALDH2*, or *dnALDH2* and exposed to hypoxia or vehicle for 2 or 24 hours. p53 expression and phosphorylation levels were examined by Western blotting using an anti-p53 or p-p53 antibody. Representative photographs from 9 samples are shown. ALDH2 expression in cultured cardiomyocytes overexpressing p53. Cultured cardiomyocytes of neonatal rats were transfected with adenoviral vectors encoding *p53* or empty vector or without transfection and exposed to anoxia or normoxia for 24 hours. mRNA or mitochondria protein was subjected respectively to reverse transcription–polymerase chain reaction (D) and Western blot (E) analyses for ALDH2 expression. Representative photograph of Western blotting is shown. β-Actin or GAPDH was used as a loading control. ALDH2 expression was quantified as folds of β-Actin or GAPDH,. Data are shown as mean±SE from 9 samples. *P<0.05 vs control with normoxia. F, 4-HNE–induced p53 phosphorylation in isolated heart. Isolated hearts were perfused with 4-HNE (10 nmol/L) or vehicle for 2 hours. Representative staining for p-p53 (brown) is shown. The p-p53 positive cells were calculated in whole LV sections and expressed as percentage of total cells. Data are shown as mean±SE of 5 hearts. *P<0.05 vs vehicle. G, Effects of a p53 inhibitor on 4-HNE–induced cardiomyocyte apoptosis. Cultured cardiomyocytes were pretreated with Pft or vehicle (negative) for 30 minutes and then incubated with 4-HNE (10 μmol/L) or vehicle for 24 hours. Apoptosis was examined by TUNEL method. Representative photographs are shown. Brown indicates the apoptotic nuclei. TUNEL-positive cells were calculated as percentage of total cells in whole dish and expressed as mean±SE of 15 samples. *P<0.01 vs respective vehicle. #P<0.05 vs 4-HNE without Pft. H, Effects of *p53* siRNA on 4-HNE–induced myocardial injury. The *p53* siRNA or a scramble control RNA (control) was injected into WT mice. The heart was isolated 2 days later and perfused with 4-HNE (10 nmol/L) or vehicle for 2 hours. Apoptosis was evaluated by TUNEL. Representative photographs are shown. Apoptotic cells were quantified as the numbers of TUNEL-positive cells per 10^4 cells in whole LV section. Data are shown as mean±SE of 5 hearts. *P<0.05 vs respective vehicle. #P<0.05 vs 4-HNE with the scramble control RNA. 4-HNE indicates 4-hydroxy-2-nonenal; ALDH2, aldehyde dehydrogenase 2; Cont, control; dnALDH2, dominant negative forms of *ALDH2*; KO, knockout; LV, left ventricle; MI, myocardial infarction; p-p53, phosphor-p53; TUNEL, terminal deoxyribonucleotide transferase–mediated dUTP nick-end labeling; Vector, empty vector; WT, wild type.

profoundly involved in the development of HF[2,21,26,32]; therefore, we examined whether modulation of ALDH2 could affect p53 expression and phosphorylation. Histological staining results showed that the protein levels of p53 were significantly increased in *ALDH2*-KO and *dnALDH2*-transfected hearts but decreased in *ALDH2*-transfected hearts compared with hearts of WT mice (Figure 11A). In addition, Western blot analysis revealed that, in response to anoxia, both the expression and phosphorylation levels of p53 in cardiomyocytes were significantly increased by *dnALDH2* but suppressed by *ALDH2* compared with empty vector transfection (Figure 11B). Another experiment under hypoxia conditions revealed the similar results to those under anoxia conditions (Figure 11C). These results suggest that ALDH2 regulates the

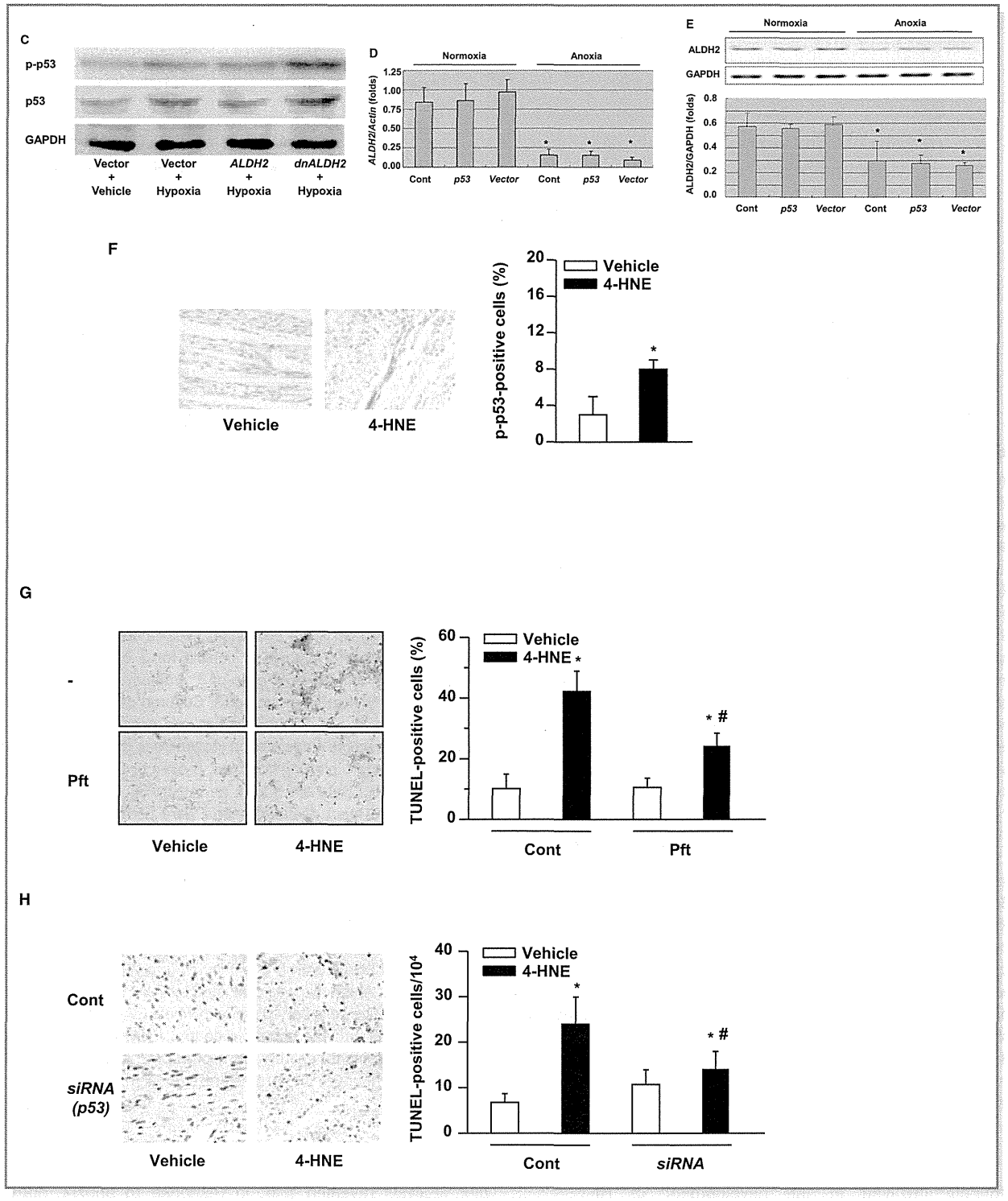

Figure 11. Continued.

expression and phosphorylation of p53 in cardiomyocytes. In turn, to understand whether p53 affects ALDH2, we examined the expression of ALDH2 after transfecting p53 into cardiomyocytes. The expression of ALDH2 at both mRNA (Figure 11D) and protein (Figure 11E) levels was not affected by transfection of p53.

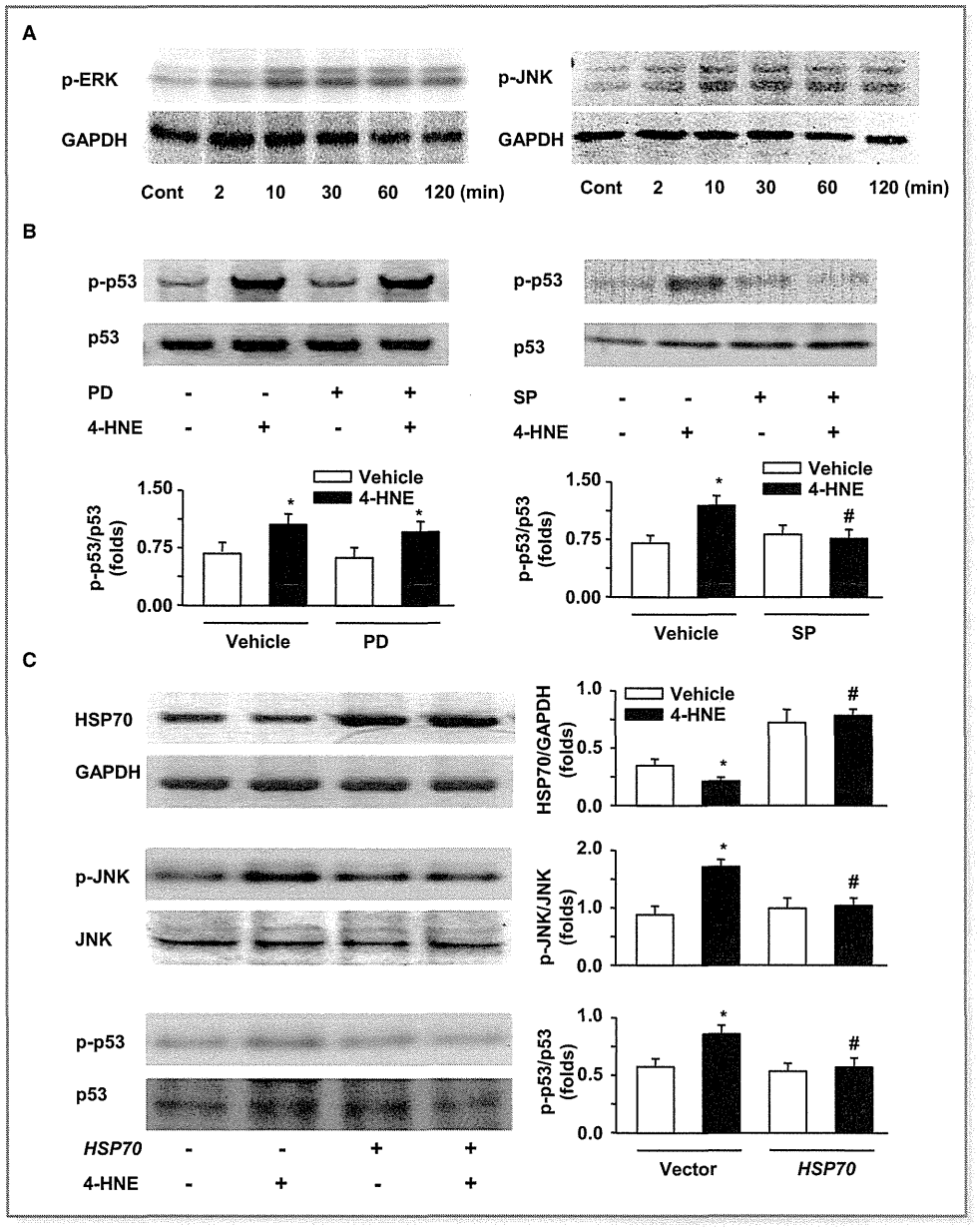

Figure 12. Involvement of HSP70 and JNK in 4-HNE–induced p53 phosphorylation. A, Western blot analysis for 4-HNE–induced time-dependent ERK or JNK phosphorylation in cultured cardiomyocytes. Cultured cardiomyocytes were stimulated with 4-HNE for the indicated times. Phosphorylations of ERKs and JNK were detected by respective antibodies. GAPDH was used as a loading control. Representative photographs are shown. B, Western blot analysis for p-p53 in cultured cardiomyocytes with or without PD or SP pretreatment. Cultured cardiomyocytes were pretreatment with PD or SP for 30 minutes and then stimulated with 4-HNE for 2 hours. p53 was used as an internal control. Representative photographs are shown. The p-p53 was quantified as folds of p53. Data are shown as mean±SE from 9 samples. *P<0.05 vs respective vehicle. #P<0.05 vs respective 4-HNE with vehicle. (C) Effects of HSP70 on 4-HNE–induced JNK and p53 phosphorylation. Cultured cardiomyocytes were transfected by an adenovirus-vector encoding HSP70 (*HSP70* +) or empty vector (*HSP70* −) for 24 hours, and then stimulated with 4-HNE (+) for 30 minutes (for p-JNK) or 2 hours (for p-p53) or with vehicle (−). GAPDH, JNK, and p53 were used as respective internal controls. Representative photographs are shown. HSP70, p-p53, and p-JNK were quantified as folds of GAPDH, JNK, and p53, respectively. Data are shown as mean±SE from 9 samples. *P<0.05 vs respective vehicle. #P<0.05 vs respective 4-HNE with vector. − indicates negative; +, positive; 4-HNE, 4-hydroxy-2-nonenal; Cont, control; p, phosphorylated; PD, PD98059; SP, SP600125; Vector, empty vector.

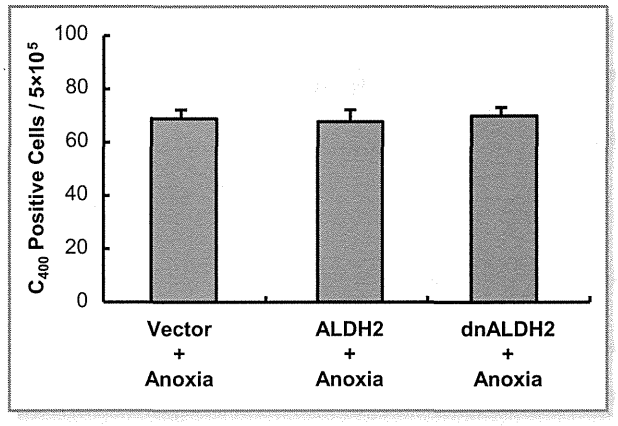

Figure 13. Effects of ALDH2 on reactive oxygen species generation in cardiomyocytes. Cultured cardiomyocytes were transfected with empty vector, *ALDH2*, and *dnALDH2* for 24 hours and exposed to anoxia for 2 hours. The cells were treated with DCFH-DA and then analyzed by a flow cytometry using excitation and emission filters of 488 and 525 nm. The increases in fluorescence emission of DCF, a derivative of DCFH-DA, reflect the enhanced cellular oxidative stress. There were no differences among 3 groups. ALDH2 indicates aldehyde dehydrogenase 2; DCF, dichlorofluorescein; DCFH-DA, 2′,7′-dichlorodihydrofluorescein diacetate. dnALDH2, dominant negative forms of *ALDH2*.

We next examined whether 4-HNE itself affected p53 expression and phosphorylation. Perfusion of the isolated heart with 4-HNE for 2 hours induced a significant increase in the phosphorylation level of p53 (Figure 11F). Treatment with Pft, a specific p53 inhibitor, significantly inhibited 4-HNE–induced apoptosis in cultured cardiomyocytes (Figure 11G). Furthermore, in vivo administration of *p53* siRNA, which efficiently suppressed the expression of p53 at both mRNA and protein levels (Figure 3A and 3B), significantly attenuated 4-HNE–induced cardiomyocyte apoptosis (Figure 11H). These results suggest that 4-HNE accumulation, a consequence of ALDH2 downregulation, could induce cardiomyocyte apoptosis through a p53-dependent pathway.

Involvement of HSP70 and JNK in 4-HNE-Induced Phosphorylation of p53

It was reported that the 2 members of MAP kinase family, the ERKs and JNK, were actively involved in the activation of p53 and apoptosis in L929 cells.[33] We explored their roles in 4-HNE stimulated cardiomyocytes. 4-HNE significantly activated both ERKs and JNK in cardiomyocytes in a time-dependent manner (Figure 12A), and pretreatment with JNK inhibitor SP600125, but not ERKs inhibitor PD98059, significantly attenuated 4-HNE–induced phosphorylation of p53 (Figure 12B), suggesting that JNK but not ERK might serve as a mediator for 4-HNE–induced p53 phosphorylation and apoptosis in cultured cardiomyocytes.

We previously reported that HSP70 suppressed the activation of JNK under hypoxia conditions in cardiomyocytes,[26] so the role of HSP70 in 4-HNE–induced phosphorylation of JNK and p53 was investigated. Our results showed that HSP70 (Figure 12C), but not HSF1 (data not shown), was

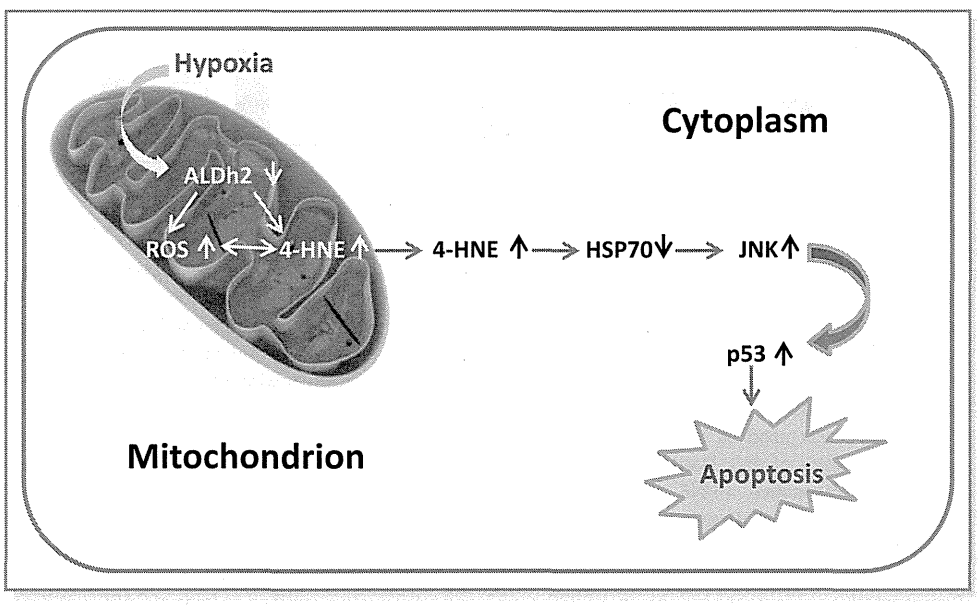

Figure 14. Proposed mechanism underlying the effects of ALDH2 on heart failure and the promising therapeutic targets. 4-HNE indicates 4-hydroxy-2-nonenal; ALDH2, aldehyde dehydrogenase 2; ROS, Reactive Oxygen Species.

significantly downregulated in 4-HNE–treated cardiomyocytes, and transfection of *HSP70* into cardiomyocytes abrogated 4-HNE–induced phosphorylation of JNK and p53 (Figure 12C). These results suggest that 4-HNE could downregulate HSP70 independently of HSF1, leading to the activation of JNK and p53 and apoptosis of cardiomyocytes.

Discussion

In the present study, downregulation of ALDH2 was identified during the development of HF after MI. Loss and gain of function of ALDH2 respectively aggravated and attenuated hypoxia-induced cardiomyocyte apoptosis and HF after MI. ALDH2 detoxifies 4-HNE, a mediator of programmed cell death events, by transmitting a mitochondrial ALDH2 signal to elicit a cytosolic response through the JNK/p53 pathway.

It has been shown that activation of mitochondrial ALDH2 by a small-molecule activator, Alda-1, reduces ischemic damage after MI in rats.[17] In this paper, we provide mechanistic insights into the homeostatic function of ALDH2 in the heart under ischemic conditions. Our present study revealed that the number of apoptotic cardiomyocytes was increased in the *ALDH2*-KO mice but was decreased by overexpression of *ALDH2* in the infarcted heart. The experiments using cultured cardiomyocytes also showed that *ALDH2*-transfected cardiomyocytes were more resistant to anoxia-induced apoptosis, whereas *dnALDH2*-transfected cardiomyocytes were more susceptible compared with mock-transfected cells. These results suggest that downregulation of ALDH2 after MI induces apoptosis of cardiomyocytes and contributes to the development of HF.

Upregulation of mitochondrial ALDH2 reduces cardiac injuries after MI through decrease of 4-HNE,[17] a finding that is consistent with our results that downregulation of ALDH2 after MI induces accumulation of 4-HNE, leading to increases in cardiomyocyte apoptosis; however, its precise mechanism, especially how 4-HNE induces cardiomyocyte death, is still unclear. A major ROS is mitochondrially derived superoxide anion radical, which attacks polyunsaturated fatty acids, leading to membrane lipid peroxidation, thereby generating reactive aldehydes including 4-HNE.[30] A previous study reported that upregulation of ALDH2 prevents apoptosis of human umbilical vein endothelial cells by decreasing ROS generation.[34] Another study showed that ALDH2 protects neuronal cells against oxidative stress by detoxifying 4-HNE rather than attenuating ROS generation.[28] In the present study, ROS was not involved in ALDH2-mediated protection of the heart during the development of HF after MI because transfection of either ALDH2 or its dominant negative mutants did not change ROS production in hypoxic cardiomyocytes (Figure 13). These results suggest that ROS is not involved in the downstream pathways of ALDH2 effects. However, transfection of ALDH2 or dnALDH2 respectively suppressed or enhanced anoxia-induced increases in 4-HNE in cardiomyocytes, indicating that ALDH2 protects cardiomyocytes, at least partially, through reducing 4-HNE.

4-HNE, a diffusible product of membrane lipid peroxidation, has been suggested as a key mediator of oxidative stress–induced cell death.[31] 4-HNE has been reported to induce upregulation and phosphorylation of p53 in retinal pigment epithelial cells.[31] Our in vitro and ex vivo experiments clearly demonstrated that 4-HNE induced functional activation of p53 and enhanced cardiomyocyte apoptosis. Either inhibition of p53 by inhibitor or knockdown of p53 by siRNA attenuated 4-HNE-induced cardiomyocyte apoptosis. These data collectively demonstrate that ALDH2-downregulation–dependent 4-HNE production after MI induces cardiomyocyte apoptosis, at least in part, through activation of the p53 pathway.

It has been unclear how 4-HNE induces functional activation of p53. In the present study, 4-HNE induced phosphorylation of JNK, and JNK inhibitor significantly suppressed 4-HNE–induced phosphorylation of p53. Although 4-HNE induced increases in the phosphorylation of ERKs, inhibition of ERKs could not suppress 4-HNE–induced phosphorylation of p53. In addition, 4-HNE could not affect the phosphorylation levels of the p38MAP kinase. These results suggest that JNK, but not ERKs or p38MAP kinase, is critical to the ALDH2/4-HNE–induced functional activation of p53. Furthermore, 4-HNE downregulated HSP70, and overexpression of HSP70 abrogated 4-HNE–induced phosphorylation of JNK and p53. Because we previously reported that HSP70 may bind to and inhibit phosphorylation of JNK,[26] our results strongly suggest that 4-HNE induced functional activation of p53, at least partially, through dowregulation of HSP70 and activation of JNK. The 4-HNE/HSP70/JNK-p53 pathway may act as an essential ALDH2 cytosolic partner, jointly participating in a coordinated multiorganelle event in the failing myocardium.

It was reported recently that overexpression of ALDH2 antagonizes chronic development of alcoholic cardiomyopathy through phosphorylation of apoptosis signal-regulating kinase 1, glycogen synthase kinase-3β, GATA binding protein 4, and cAMP response-element binding protein.[18] The data from same group also indicated that ALDH2 overexpression antagonizes chronic alcohol intake–induced cardiac insulin insensitivity and contractile defect via improvement of insulin signaling at the levels of insulin receptor, insulin receptor substrate, protein kinase B/Akt, Foxo3a, and JNK.[34] Quite recently, proinflammatory cytokine macrophage migration inhibitory factor has been shown to regulate mammalian target of rapamycin signaling to activate autophagy to preserve cardiac geometry and protect against cardiac injuries.[36] Whether these proteins take part in the mecha-

nistic event in our present post-MI setting needs to be addressed in a future study.

In summary, our results suggest that ischemic injury could result in downregulation of mitochondrial ALDH2 in mice hearts after MI, leading to 4-HNE accumulation. The increased 4-HNE transmits the mitochondrial signal to cytosol, enhancing cardiomyocyte apoptosis through downregulation of HSP70 and activation of JNK and p53, and thereby promotes the development of HF (Figure 14). Enhancing myocardial ALDH2 expression or activity might emerge as a promising therapeutic strategy for HF.

Acknowledgments

We thank Dr Shigeo Ohta at Nippon Medical School, Tokyo, Japan, for kindly providing the *ALDH2* plasmids. We thank Jianguo Jia and Bingyu Li at Zhongshan Hospital and Guoping Zhang at Institute of Biomedical Science, Fudan University, Shanghai, China, for technical assistance.

Sources of Funding

Key Program of National Natural Science Foundation of China (30930043), National Natural Science Foundation of China (30971250), National Basic Research Program of China (2007CB512003), China Doctoral Foundation (20110071110051), the Science and Technology Commission of Shanghai Municipality (11JC1402400).

Disclosures

None.

References

1. Cleland JG, Khand A, Clark A. The heart failure epidemic: exactly how big is it. *Eur Heart J*. 2001;22:623–626.
2. Kociol RD. Most important papers in pathophysiology and genetics. *Circ Heart Fail*. 2012;5:32–49.
3. Goffart S, von Kleist-Retzow JC, Wiesner RJ. Regulation of mitochondrial proliferation in the heart: power-plant failure contributes to cardiac failure in hypertrophy. *Cardiovasc Res*. 2004;64:198–207.
4. Huss JM, Kelly DP. Mitochondrial energy metabolism in heart failure: a question of balance. *J Clin Invest*. 2005;115:547–555.
5. Giordano FJ. Oxygen, oxidative stress, hypoxia, and heart failure. *J Clin Invest*. 2005;115:500–508.
6. Gong G, Liu J, Liang P, Guo T, Hu Q, Ochiai K, Hou MX, Ye Y, Wu XY, Mansoor A, From AHL, Ugurbil K, Bache RJ, Zhang JY. Oxidative capacity in failing hearts. *Am J Physiol Heart Circ Physiol*. 2003; 285:H541–H548.
7. Grieve DJ, Shah AM. Oxidative stress in heart failure. More than just damage. *Eur Heart J*. 2003;4:2161–2163.
8. Kocher AA, Schuster MD, Szabolcs MJ, Takuma S, Burkhoff D, Wang J, Homma S, Edwards NM, Itescu S. Neovascularization of ischemic myocardium by human bone-marrow-derived angioblasts prevents cardiomyocyte apoptosis, reduces remodeling and improves cardiac function. *Nat Med*. 2001;7:430–436.
9. Crow MT, Mani K, Nam YJ, Kitsis RN. The mitochondrial death pathway and cardiac myocyte apoptosis. *Circ Res*. 2004;95:957–970.
10. Regula KM, Kirshenbaum LA. Apoptosis of ventricular myocytes: a means to an end. *J Mol Cell Cardiol*. 2005;38:3–13.
11. Wencker D, Chandra M, Nguyen K, Miao W, Garantziotis S, Factor SM, Shirani J, Armstrong RC, Kitsis RN. A mechanistic role for cardiac myocyte apoptosis in heart failure. *J Clin Invest*. 2003;111:1497–1504.
12. Chen Z, Zhang J, Stamler JS. Identification of the enzymatic mechanism of nitroglycerin bioactivation. *Proc Natl Acad Sci USA*. 2003;99:8306–8311.
13. Mackenzie IS, Maki-Petaja KM, McEniery CM, Bao YP, Wallace SM, Cheriyan J, Monteith S, Brown MJ, Wilkinson IB. Aldehyde dehydrogenase 2 plays a role in the bioactivation of nitroglycerin in humans. *Arterioscler Thromb Vasc Biol*. 2005;25:1891–1895.
14. Chen Z, Foster MW, Zhang J, Mao L, Rockman HA, Kawamoto T, Kitagawa K, Nakayama KI, Hess DT, Stamler JS. An essential role for mitochondrial aldehyde dehydrogenase in nitroglycerin bioactivation. *Proc Natl Acad Sci USA*. 2005;102:12159–12164.
15. Li Y, Zhang D, Jin W, Shao C, Yan P, Xu C, Sheng H, Liu Y, Yu J, Xie Y, Zhao Y, Lu D, Nebert DW, Harrison DC, Huang W, Jin L. Mitochondrial aldehyde dehydrogenase-2 (ALDH2) Glu504Lys polymorphism contributes to the variation in efficacy of sublingual nitroglycerin. *J Clin Invest*. 2006;116:506–511.
16. Oyama T, Isse T, Ogawa M, Muto M, Uchiyama I, Kawamoto T. Susceptibility to inhalation toxicity of acetaldehyde in Aldh2 knockout mice. *Front Biosci*. 2007;12:1927–1934.
17. Chen CH, Budas GR, Churchill EN, Disatnik MH, Hurley TD, Mochly-Rosen D. Activation of aldehyde dehydrogenase-2 reduces ischemic damage to the heart. *Science*. 2008;321:1493–1495.
18. Doser TA, Turdi S, Thomas DP, Epstein PN, Li SY, Ren J. Transgenic overexpression of aldehyde dehydrogenase-2 rescues chronic alcohol intake-induced myocardial hypertrophy and contractile dysfunction. *Circulation*. 2009;119:1941–1949.
19. Fan F, Sun A, Zhao H, Liu X, Zhang W, Jin X, Wang C, Ma X, Shen C, Zou Y, Hu K, Ge J. MicroRNA-34a promotes cardiomyocyte apoptosis post myocardial infarction through down-regulating aldehyde dehydrogenase 2. *Curr Pharm Des*. 2013;19:4865–4873.
20. Isse T, Oyama T, Matsuno K, Ogawa M, Narai-Suzuki R, Yamaguchi T, Murakami T, Kinaga T, Uchiyama I, Kawamoto T. Paired acute inhalation test reveals that acetaldehyde toxicity is higher in aldehyde dehydrogenase 2 knockout mice than in wild-type mice. *J Toxicol Sci*. 2005;30:329–337.
21. Sano M, Minamino T, Toko H, Miyauchi H, Orimo M, Qin Y, Akazawa H, Tateno K, Kayama Y, Harada M, Shimizu I, Asahara T, Hamada H, Tomita S, Molkentin JD, Zou Y, Komuro I. p53-induced inhibition of Hif-1 causes cardiac dysfunction during pressure overload. *Nature*. 2007;446:444–448.
22. Zou Y, Li J, Ma H, Jiang H, Yuan J, Gong H, Liang Y, Guan A, Wu J, Li L, Zhou N, Niu Y, Sun A, Nakai A, Wang P, Takano H, Komuro I, Ge J. Heat shock transcription factor 1 protects heart after pressure overload through promoting myocardial angiogenesis in male mice. *J Mol Cell Cardiol*. 2011;51:821–829.
23. Hilfiker-Kleiner D, Hilfiker A, Kaminski K, Schaefer A, Park JK, Michel K, Quint A, Yaniv M, Weitzman JB, Drexler H. Lack of JunD promotes pressure overload-induced apoptosis, hypertrophic growth, and angiogenesis in the heart. *Circulation*. 2005;112:1470–1477.
24. Yin C, Xi L, Wang X, Eapen M, Kukreja RC. Silencing heat shock factor 1 by small interfering RNA abrogates heat shock-induced cardioprotection against ischemia-reperfusion injury in mice. *J Mol Cell Cardiol*. 2005;39:681–689.
25. National Research Council (US) Institute for Laboratory Animal Research. Guide for the Care and Use of Laboratory Animals. Washington (DC): National Academies Press (US); 1996.
26. Harada M, Qin Y, Takano H, Minamino T, Zou Y, Toko H, Ohtsuka M, Matsuura K, Sano M, Nishi J, Iwanaga K, Akazawa H, Kunieda T, Zhu W, Hasegawa H, Kunisada K, Nagai T, Nakaya H, Yamauchi-Takihara K, Komuro I. G-CSF prevents cardiac remodeling after myocardial infarction by activating the Jak-Stat pathway in cardiomyocytes. *Nat Med*. 2005;11:305–311.
27. Zou Y, Zhu W, Sakamoto M, Qin Y, Akazawa H, Toko H, Mizukami M, Takeda N, Minamino T, Takano H, Nagai T, Nakai A, Komuro I. Heat shock transcription factor 1 protects cardiomyocytes from ischemia/reperfusion injury. *Circulation*. 2003;108:3024–3030.
28. Ohsawa I, Nishimaki K, Yasuda C, Kamino K, Ohta S. Deficiency in a mitochondrial aldehyde dehydrogenase increases vulnerability to oxidative stress in PC12 cells. *J Neurochem*. 2003;84:1110–1117.
29. Fujimoto M, Takaki E, Hayashi T, Kitaura Y, Tanaka Y, Inouye S, Nakai A. Active HSF1 significantly suppresses polyglutamine aggregate formation in cellular and mouse models. *J Biol Chem*. 2005;280:34908–34916.
30. Bhatnagar A. Electrophysiological effects of 4-hydroxynonenal, an aldehydic product of lipid peroxidation, on isolated rat ventricular myocytes. *Circ Res*. 1995;76:293–304.

31. Sharma A, Sharma R, Chaudhary P, Vatsyayan R, Pearce V, Jeyabal PVS, Zimniak P, Awasthi S, Awasthi YC. 4-Hydroxynonenal induces p53-mediated apoptosis in retinal pigment epithelial cells. *Arch Biochem Biophys*. 2008;480:85–94.

32. Moorjani N, Catarino P, Trabzuni D, Saleh S, Mooji A, Dzimiri N, Al-Mohanna F, Westaby S, Ahmad M. Upregulation of Bcl-2 proteins during the transition to pressure overload-induced heart failure. *Int J Cardiol*. 2007; 116:27–33.

33. Cheng Y, Qiu F, Tashiro S, Onodera S, Ikejima T. ERK and JNK mediate TNFalhpa-induced p53 activation in apoptotic and autophagic L929 cell death. *Biochem Biophys Res Commun*. 2008;376:483–488.

34. Li SY, Gomelsky M, Duan JH, Zhang ZJ, Gomelsky L, Zhang XC, Epstein PN, Ren J. Overexpression of aldehyde dehydrogenase-2 (ALDH2) transgene prevents acetaldehyde-induced cell injury in human umbilical vein endothelial cells: role of ERK and p38 mitogen-activated protein kinase. *J Biol Chem*. 2004;279:11244–11252.

35. Li SY, Gilbert SA, Li Q, Ren J. Aldehyde dehydrogenase-2 (ALDH2) ameliorates chronic alcohol ingestion-induced myocardial insulin resistance and endoplasmic reticulum stress. *J Mol Cell Cardiol*. 2009;47:247–255.

36. Xu X, Hua Y, Nair S, Bucala R, Ren J. Macrophage migration inhibitory factor deletion exacerbates pressure overload-induced cardiac hypertrophy through mitigating autophagy. *Hypertension*. 2014;63:490–499.

Am J Physiol Heart Circ Physiol 307: H1339–H1352, 2014.
First published August 29, 2014; doi:10.1152/ajpheart.01021.2013.

Effects of methylglyoxal on human cardiac fibroblast: roles of transient receptor potential ankyrin 1 (TRPA1) channels

Gaku Oguri,[1] Toshiaki Nakajima,[2] Yumiko Yamamoto,[1] Nami Takano,[1] Tomofumi Tanaka,[1] Hironobu Kikuchi,[1] Toshihiro Morita,[2] Fumitaka Nakamura,[4] Tatsuya Yamasoba,[3] and Issei Komuro[1]

[1]*Department of Cardiovascular Medicine, University of Tokyo, Tokyo, Japan;* [2]*Department of Ischemic Circulatory Physiology, University of Tokyo, Tokyo, Japan;* [3]*Department of Otolaryngology, University of Tokyo, Tokyo, Japan; and* [4]*Teikyo University Chiba Medical Center, Ichihara, Chiba, Japan*

Submitted 28 December 2013; accepted in final form 6 August 2014

Oguri G, Nakajima T, Yamamoto Y, Takano N, Tanaka T, Kikuchi H, Morita T, Nakamura F, Yamasoba T, Komuro I. Effects of methylglyoxal on human cardiac fibroblast: roles of transient receptor potential ankyrin 1 (TRPA1) channels. *Am J Physiol Heart Circ Physiol* 307: H1339–H1352, 2014. First published August 29, 2014; doi:10.1152/ajpheart.01021.2013.—Cardiac fibroblasts contribute to the pathogenesis of cardiac remodeling. Methylglyoxal (MG) is an endogenous carbonyl compound produced under hyperglycemic conditions, which may play a role in the development of pathophysiological conditions including diabetic cardiomyopathy. However, the mechanism by which this occurs and the molecular targets of MG are unclear. We investigated the effects of MG on Ca^{2+} signals, its underlying mechanism, and cell cycle progression/cell differentiation in human cardiac fibroblasts. The conventional and quantitative real-time RT-PCR, Western blot, immunocytochemical analysis, and intracellular Ca^{2+} concentration $[Ca^{2+}]i$ measurement were applied. Cell cycle progression was assessed using the fluorescence activated cell sorting. MG induced Ca^{2+} entry concentration dependently. Ruthenium red (RR), a general cation channel blocker, and HC030031, a selective transient receptor potential ankyrin 1 (TRPA1) antagonist, inhibited MG-induced Ca^{2+} entry. Treatment with aminoguanidine, a MG scavenger, also inhibited it. Allyl isothiocyanate, a selective TRPA1 agonist, increased Ca^{2+} entry. The use of small interfering RNA to knock down TRPA1 reduced the MG-induced Ca^{2+} entry as well as TRPA1 mRNA expression. The quantitative real-time RT-PCR analysis showed the prominent existence of TRPA1 mRNA. Expression of TRPA1 protein was confirmed by Western blotting and immunocytochemical analyses. MG promoted cell cycle progression from G0/G1 to S/G2/M, which was suppressed by HC030031 or RR. MG also enhanced α-smooth muscle actin expression. The present results suggest that methylglyoxal activates TRPA1 and promotes cell cycle progression and differentiation in human cardiac fibroblasts. MG might participate the development of pathophysiological conditions including diabetic cardiomyopathy via activation of TRPA1.

human cardiac fibroblast; transient receptor potential ankyrin 1 channels; methylglyoxal

CARDIAC FIBROBLASTS ARE THE predominant secretary cell types located within the extracellular matrix (ECM) (18), which account for 60~70% of the cells in human hearts and play a key role in regulating normal myocardial function and in the adverse myocardial remodeling that occurs with hypertension, heart failure, and myocardial infarction (12, 71). Many of the functional effects of cardiac fibroblasts are mediated through differentiation of cardiac fibroblasts to myofibroblasts phenotype that expresses contractile proteins such as α-smooth muscle actin (α-SMA), and they consequently exhibit increased migratory and proliferative properties. Cardiac fibroblasts also take a part in the maintenance of myocardial function by producing the type I and type III collagens and by secreting growth factors (48), and a key source of components of the ECM that regulates the structure of the heart and hence mechanical, chemical, and electrical signals between cellular and noncellular components (54). Thus cardiac fibroblasts play an essential role in the fibrosis and remodeling by increased proliferation (4) and elevated collagen production (61) under the various pathophysiological conditions such as diabetic cardiomyopathy (41).

Methylglyoxal (MG) is a highly reactive dicarbonyl metabolite produced during glucose metabolism (23). MG levels mediate rapid nonenzymatic glycation of proteins and other substrates, promoting formation of advanced glycation end (AGE) products, which are involved in the pathogenesis of vascular complications of diabetes (7), (23). AGEs and AGEs receptor (RAGE) cause inflammation, apoptosis, oxidative stress, gene transcription, atherogenesis, and impaired angiogenesis. In addition, MG can react with and modifies certain proteins, lipids, and DNA and alters their normal structure and/or function (7, 23). It has been reported that MG levels were elevated in spontaneously hypertensive rats (68) and in diabetic patients (65) since hyperglycemia strongly enhances MG accumulation (8, 45). In vitro studies also showed that incubation of vascular smooth muscle cells (VSMCs) with high glucose or fructose for 3 h increased MG production 3.5- or 3.9-fold, respectively, and increased oxidative stress (24).

Diabetic cardiomyopathy is a diabetic complication and a risk of heart failure (HF) (10) defined as ventricular dysfunction that occurs in diabetic patients independent of a recognized cause (e.g., coronary heart disease, hypertension). Diastolic dysfunction is a functional character in diabetic cardiomyopathy (27), (57). AGE product deposition has been reported to increase LV diastolic stiffness directly by cross-linking collagen, indirectly by enhancing collagen formation or reducing nitric oxide bioavailability (33, 63). Recently, Shao et al. (56) showed that MG reduced the ability of sarco(endo) plasmic reticulum Ca^{2+}-ATPase 2a to transport Ca^{2+} and induced diastolic dysfunction, which may play a role in development of diabetic cardiomyopathy. In addition, MG has been reported to affect cardiac fibroblasts function by promoting myofibroblast differentiation (74), but the mechanism by which this occurs and the molecular targets of MG are unclear.

The transient receptor potential (TRP) channel superfamily consists of 28 mammalian cation channels and is expressed in

Address for reprint requests and other correspondence: T. Nakajima, Dept. of Ischemic Circulatory Physiology, Univ. of Tokyo, 7-3-1 Hongo, Bunkyo-ku, Tokyo, Japan (e-mail: nakajima-2im@h.u-tokyo.ac.jp).

almost tissue, including the heart. Most TRP channels are permeable to Ca^{2+} and are prime molecular candidates for store-operated channels, receptor-operated channels, ligand-gated channels, and stretch-activated channels. In the whole heart, the expression of several TRP channels has been demonstrated in RT-PCR or biochemical studies (31, 36). These TRP channels act as multifunctional cellular sensors and have several fundamental cell functions such as contraction, proliferation, and secretion. Among TRP channel family, several studies have revealed the involvement of TRP channels (TRPCs) on cardiac hypertrophy and remodeling (31, 44, 72). Cardiac fibroblasts also contribute to the pathogenesis of cardiac remodeling, and the existence of TRPC1, 3, 4, and 6 has been reported by RT-PCR analysis in cardiac fibroblasts (17, 25, 35). Treatment with TGF-β1 has been reported to increase the Ca^{2+} influx via activation of TRP channels (TRPM7, TRPC1, and TRPC6) (25, 35). Davis et al. (22) showed an obligate function for TRPC6 in promoting myofibroblast differentiation and wound healing in mice, whereas Harada et al. (32) reported the essential role of TRPC3 on rat cardiac fibroblast proliferation and differentiation. The function and existence of TRPV1, TRPV2, and TRPV4 have also been reported in cardiac fibroblasts and myocytes (34, 42, 75).

Alternatively, the TRP ankyrin channel (TRPA) is also a member of the large TRP family of ion channels and functions as a Ca^{2+} permeable nonselective cation channel. The only mammalian TRPA subfamily member, TRPA1, is widely expressed in peripheral and central termini of small diameter primary afferent neurons and the ganglia of these dorsal, trigeminal, and nodose neurons (6, 59), and nonneuronal cells including epithelial cells (49). Based on localization and functional properties, TRPA1 is considered a key player in acute and chronic (neuropathic) pain and inflammation and integrates the nociception of a large variety of different, potentially damaging and noxious stimuli: cold (40, 59) and electrophilic compounds (6, 38). Diabetic neuropathy is one of diabetic complication. And it has been reported that a rise in serum MG density participates in diabetic neuropathy directly (9), and MG activates nociceptors through TRPA1 in diabetic neuropathy (26, 53). Thus it is likely that MG may play a role in diabetic complication such as neuropathy. Therefore, it is interesting to investigate the molecular target of MG and involvement of TRPA1 on human cardiac fibroblasts.

The purpose of the present study is to investigate the expression and function of TRPA1 and the effects of MG on Ca^{2+} signals, fibroblast proliferation, and differentiation in human cardiac fibroblasts. We show that MG activates TRPA1 and promotes cell cycle progression and differentiation in human cardiac fibroblasts.

MATERIALS AND METHODS

Cell culture of human cardiac fibroblasts. Human adult ventricular cardiac fibroblasts (ACBRI 5118) were purchased from DS Pharma Biomedical (Osaka, Japan). Cells were maintained at 37°C under 5% CO_2 in Cell System containing 10% serum and defined cell boost (CSC Catalog 4ZO-50). At confluence, the cells were detached using 0.25% trypsin in 0.02% EDTA and cultured into the medium. Medium was replaced more than twice weekly. Cells before confluence at passage 3–6 were detached from culture dish with 0.25% trypsin in 0.02% EDTA and used for later experiments.

Solutions and drugs. MG was purchased from Nakarai Tesque (Kyoto, Japan). HC030031 [2-(1,3-dimethyl-2,6-dioxo-1,2,3,6-tetrahydro-7H-purin-7-yl)-N-(4-isopropylphenyl)acetamide], a selective TRPA1 blocker, was purchased from Abcam Biochemicals (Cambridge, UK). Ruthenium red, a general cation channel blocker, and allyl isothiocyanate (AITC), a selective TRPA1 agonist (38), and 15-deoxy-delta-12, 14-prostaglandin J2 (15d-PGJ2) were purchased from Wako Pure Chemical Industries (Osaka, Japan). Nicardipine, aminoguanidine, dithiothreitol (DTT), and fura-2 acetoxymethyl ester (fura-2 AM) were purchased from Sigma-Aldrich (Poole, UK). LY2157299, a potent and selective TGF-β_1 receptor blocker, was purchased from AdooQ BioScience.

Measurement of intracellular Ca^{2+} concentration $[Ca^{2+}]_i$. Cytosolic free Ca^{2+} concentration ($[Ca^{2+}]_i$) was determined using the fluorescence method as described previously (30, 52). Human cardiac fibroblasts were trypsinized, washed twice in the standard solution, adjusted to a cell density of 10^6 cells ml-1 and loaded with 2 μM fura-2 AM for 30 min at 37°C under 5% CO_2. After incubation, the medium containing fura-2 AM was removed, and fluorescent cells in suspensions were measured at 37°C while stirred continuously in a cuvette placed by a spectrofluorometer (CAF-100; Jasco, Tokyo, Japan). The excitation wavelengths were 340 and 380 nm, and emission was 500 nm. In the evaluation of Ca^{2+} responses, the amplitude of Ca^{2+} elevation in response to each stimulant was calculated by the increase of F340/F380 with reference to the value at the resting state. In experiments of HC030031, ruthenium red, or DTT, we added them 1 min before the application of Ca^{2+} into the bath solution.

Immunocytochemistry. Immunocytochemistry was performed on human cardiac fibroblasts using anti-TRPA1 channels antibodies (Novus Biologicals) or anti-α-smooth muscle actin (SMA) (Cy3-conjugated anti-α-actin; Sigma). The cells were cultured on Lab-Tek collagen-coated chamber slide (Nalge Nunc International, Naperville, IL), fixed with 2% paraformaldehyde in PBS in 20 min, and then blocked for 15 min with 2% horse serum and 0.1% saponin in PBS. The cells were incubated for 1 h with primary antibodies diluted with 0.01% Triton X and 0.01% NaN3 in PBS into 1:200–1:1,000. For negative controls, cells were treated with normal Rabbit IgG. Alexa Fluor 555 labeled Goat anti-rabbit IgG antibody diluted 1:1,000 (Molecular Probes; A21428) was used to visualize the channel expression. The cells were also stained with 2-(4-amidinophenyl)-1H-indole-6-carboxamidine (DAPI) to visualize nuclei. A confocal laser scanning microscopy (Olympus Fluo View FV300; Olympus) was used for observations.

RNA extraction, RT-PCR, and real-time quantitative RT-PCR. To determine the expression of TRP channel in human cardiac fibroblasts by RT-PCR, total cellular RNA was extracted from the cultured cells by using the RNeasy mini kit (Qiagen, Cambridge, MA). For RT-PCR, complementary DNA (cDNA) was synthesized from 1 μg of total RNA with reverse transcriptase with random primers (Toyobo, Osaka, Japan). The reaction mixture was then subjected to PCR amplification with specific forward and reverse oligonucleotide primers for 35 cycles consisting of heat denaturation, annealing, and extension. The cycling conditions were denaturation at 98°C for 20 s, annealing at 52–56°C for 10 s, and extension at 74°C for 1 min. PCR products were size-fractionated on 2% agarose gels and stained with ethidium bromide and visualized under UV light. The forward and reverse primer sequences for TRPA1 were 5′-TGGTGCACAA-ATAGACCCAGT-3′ and 5′-TGGGCACCTTTAGAGAGTAGC -3′. The forward and reverse primer sequences for GAPDH were 5′-GAGTCAACGGATTTGGTCGT -3′ and 5′-TGACAAAGTGGTC-GTTGAGG -3′.

Real-time quantitative RT-PCR was performed with the use of real-time Taq-Man technology and a sequence detector (ABI PRISM7000; Applied Biosystems, Foster City, CA). Gene-specific primers and Taq-Man probes were used to analyze transcript abundance. The 18S ribosomal RNA level was analyzed as an internal

control and used to normalize the values for transcript abundance of TRP family genes. The probes used in this study ware purchased as Assay-on-Demand from Applied Biosystems (Foster City, CA): assay ID Hs00175798_m1 for TRPA1, assay ID Hs00608195_m1 for TRPC1, assay ID Hs01066071 _m1 for TRM2, assay ID Hs00218912 _m1 for TRPV1, assay ID Hs00901640_m1 for TRPV2, and assay ID 4310893E for 18S rRNA endogenous control.

Western blotting. Proteins were separated on a 10% polyacrylamide gel for 60 min at 200 V and then transferred to Amersham Hypond-P (GE Healthcare UK, Buckinghamshire, England) for 60 min at 72 mA with semi-dry method. After the transfer, the membrane was blocked with Blocking One (Nakarai Tesque, Kyoto, Japan) at room temperature for 1 h. The membrane was then exposed to anti-TRPA1 antibodies (Novus Biologicals, Littleton, CO) or anti-α-SMA (Cy3-conjugated anti-α-actin; Sigma) at the dilutions in blocking buffer overnight at 4°C. Probed membrane was then washed three times in PBS-T for 15 min each time and subsequently incubated with anti-rabbit IgG linked to peroxidase (Santa Cruz Biotechnology) diluted to 1:5,000 with blocking buffer for 1 h at room temperature. After three additional washes, bound antibodies were detected by Chemi-Lumi One Super (Nacalai Tesque, Kyoto, Japan) and analyzed with an LAS-3000 mini image analyzer (Fuji-Film, Tokyo, Japan).

Transfection of synthetic small interfering RNA. TRPA1 small interfering RNA (siRNA; Sense: ACGAAUUCAUAUCUAA-UAATT; Antisense: UUAUUAGAUAUGAAUUCCGUGG) and nonsilencing siRNA (negative control; Allstars Negative control) were purchased from Qiagen (Cambridge, MA). They were transfected into human cardiac fibroblasts to a final concentration of 24 nmol/l, by using the Lipofectamine RNAiMAX Transfection Reagent (10 ml/ml culture; Life Technologies, Carlsbad, CA) according to the instructions of the manufacturer. Transfected cells were incubated for 48 h in an atmosphere of 5% CO_2 and 95% air at 37°C before each experiment. Analysis of mRNA by using real-time RT-PCR and the functions of the cells were then performed. Rhodamine-conjugated siRNA was used to confirm the transfection of siRNA by using Nikon ECLISE TE200-u.

Cell-cycle analysis using flow cytometry. Human cardiac fibroblasts were plated about 5,000 cells/cm^2 into 6-cm dishes, after saved in serum-free media for 24 h, and in the presence or absence of methylglyoxal (300 μM) or drugs for 48 h at 37°C, 5% CO_2. After 48 h incubation, cells were totally washed in PBS (Wako Pure Chemical Industries, Osaka, Japan) and harvested from all dishes following trypsinization. Cells were then mixed in 500 μl of PBS contained 3% FBS and 0.05% NaN_3 and centrifuged. And cells were added 5 ml of ice-cold 70% ethanol and resuspended and incubated at room temperature for 30 min. They were then again centrifuged and added PBS contained 0.05 mg/ml Ribonuclease A (Sigma-Aldrich) and 0.01 mg/ml propidium iodide (PI; Sigma-Aldrich). The final volume in each sample was 600 μl. In each preparation, the numbers of cells and PI fluorescence were measured with a Guva easycyteplus (Merck Millipore, Billerica, MA) at 680 nm emission-wavelength to create a DNA content-frequency histogram. Samples were gated on fibroblast population stained PI. The percentage of cells in each phase of the cell cycle, G0/G1, S, and G2/M phases, was analyzed using Cytosoft 5.3 of Merck Millipore.

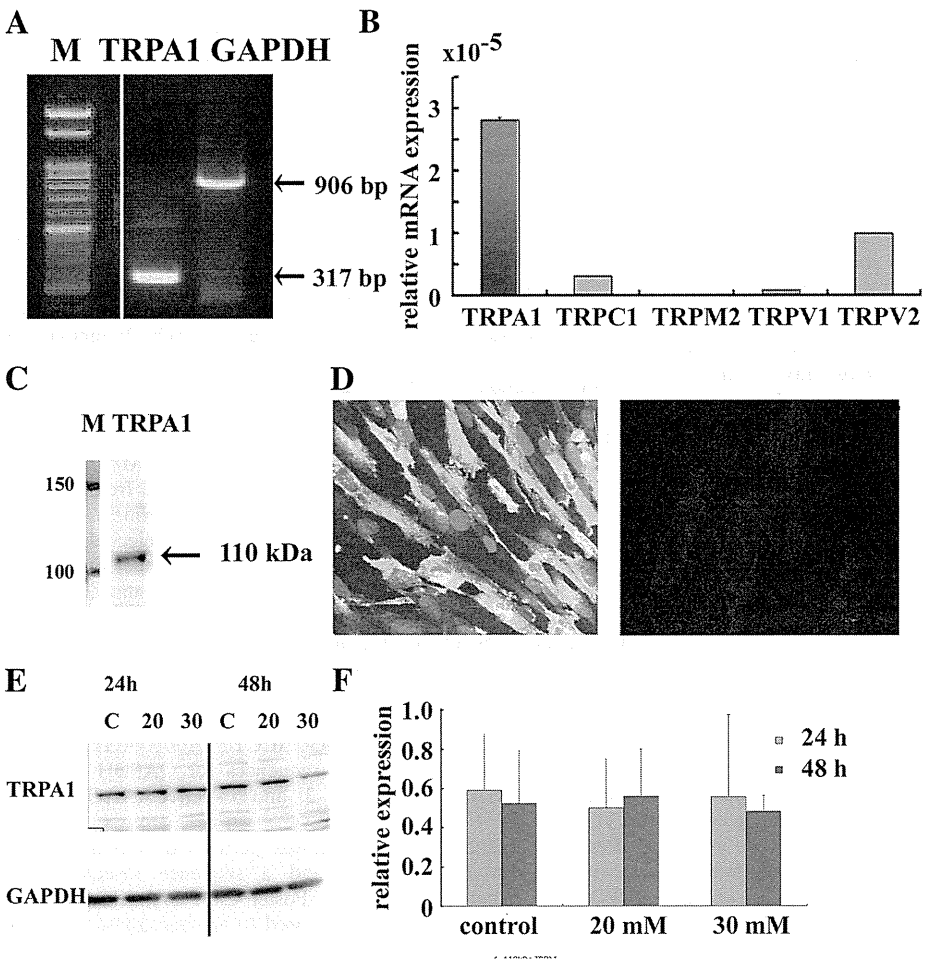

Fig. 1. Transient receptor potential ankyrin 1 (TRPA1) expression in human cardiac fibroblasts. *A*: expression of α subunit gene of TRPA1 channel in human cardiac fibroblasts. Marker, M; GAPDH, used as a loading control. *B*: quantitative real-time RT-PCR analysis of TRPA1, TRPC1, TRPM2, TRPV1, and TRPV2 in human cardiac fibroblasts. The expression levels of TRP channel genes were normalized to those of the 18S ribosomal RNA levels. Note that dominant expression of TRPA1 mRNA was observed in human cardiac fibroblasts. *C*: Western blotting for TRPA1 (indicated by an arrow). *D*: immunostaining for TRPA1. Negative control without the antibody (right part). Double staining of nuclei DAPI to visualize nuclei is illustrated. Note that human cardiac fibroblasts have significant expression for TRPA1. *E* and *F*: effects of high glucose (20 and 30 mM) on TRPA1 expression. The cells were treated with 5.4 mM (control solution), 20 mM, and 30 mM (high glucose solution) for 24 h and 48 h. The TRPA1 protein expression was measured by Western blotting, and the ratio of TRPA1 optical density to the corresponding GAPDH optical density is shown in *F*. Each data represents the mean ± SD of paired 3 different experiments.